UNIVERSITAT POLITÈCNICA DE CATALUNYA
BARCELONATECH
Escola Superior d'Enginyeries Industrial,
Aeroespacial i Audiovisual de Terrassa

BACHELOR FINAL THESIS

Evaluation of Geostationary Lightning Mapper performance using the Colombia-Lightning Mapping Array

Document:

Bachelor Final Thesis Report

Author:

Mar Borràs Farnós

Director/Co-director:

Joan Montanyà Puig

Jesús Alberto López Trujillo

Degree:

Bachelor in Aerospace Engineering

Examination session:

June 22, 2022

Abstract

The Geostationary Lightning Mapper (GLM) on the Geostationary Operational Environmental Satellites - R (GOES-R) series satellites is the first operational lightning mapper flown in a geostationary orbit, which provides continuous observations of lightning. In order to make use of these data for improving nowcasting of severe weather and for data assimilation, it is important to characterize and understand the detection capabilities of GLM. Observations from 3-dimensional VHF Colombia Lightning Mapping Arrays (COL-LMA) provide a valuable basis for evaluating the spatial accuracy and detection efficiencies of observations from the recently launched, optical-based Geosynchronous Lightning Mapper (GLM). This Bachelor Final Thesis results of comparing spatially and temporally the individual event (pixel) level for sets of individual discharges from the LMA and GLM observations. The focus is on a representative sample of case studies encompassing different forms of convective organization at different times of day and night. The detection efficiency of GLM relative to LMA will be characterized in terms of the flash number, size, power and height among others.

Keywords: Geostationary Lightning Mapper (GLM), Colombia Lightning Mapping Array (COL-LMA), Lightning, Detectors.

Resum

El Gestationary Lightning Mapper (GLM), incorporat dins la constel·lació de satèl·lits Geostationary Operational Environmental Satellites - R (GOES-R), és el primer mapejador de llamps operatiu en una òrbita geoestacionària i que proporciona observacions contínues dels raigs. Per utilitzar aquestes dades per tal de millorar la previsió de temps sever i per a l'assimilació de dades, és important caracteritzar i comprendre les capacitats de detecció del GLM. Les observacions dels conjunts tridimensionals del sensor d'alta freqüència del Colòmbia Lightning Mapping Array (COL-LMA) proporcionen una base valuosa per avaluar la precisió espacial i l'eficiència de detecció de les observacions del recentment llançat Geosynchronous Lightning Mapper (GLM). En aquest Treball de Fi de Grau es comparen espacialment i temporalment els nivells d'event individual (píxel) per a conjunts de descàrregues elèctriques a través de les observacions del LMA i el GLM. L'enfocament que se li dona en aquest projecte és en una mostra representativa de diferents casos d'estudi abastant diferents formes d'organització convectiva en diferents moments del dia i la nit. L'eficiència de detecció del GLM en relació amb el LMA es caracteritzarà en termes del nombre de llamps, de la mida, de la potència i de l'alçada, entre d'altres.

Paraules Clau: Geostationary Lightning Mapper (GLM), Colòmbia Lightning Mapping Array (COL-LMA), Llamps, Detectors.

Acknowledgements

To the director and co-director of this thesis, Joan Montanyà and Jesús López, for offering me the opportunity to learn about the fascinating domain of lightning in the Lightning Research Group, for all the time dedicated and for the excellent treatment and attention they offered me during the elaboration of this project.

To my family; specially to my mother, who has always helped me, who has given me strength in the bad times and who has educated me in the values to become the person I am today. All I do is because of you. I miss you everyday.

To the amazing people I met during these four years in the university who have supported and helped me the most in the hardest moments when I most wanted to give up.

To my friends who have made me feel loved, who have encouraged me to achieve my goals and with whom I have shared unforgettable experiences.

To everyone who has contributed in any way to help me get to this point.

My sincerest thank you.

Contents

List of Figures

List of Tables

List of abbreviations

GLM - Geostationary Lightning Mapper

MTG - Meteosat Third Generation

LMA - Lightning Mapping Array

COL-LMA - Colombia-Lightning Mapping Array

GCR - Galactic Cosmic Rays

GEC - Global Earth Circuit

CG - Cloud-to-Ground

CC - Cloud-to-Cloud

IC - Intra-Cloud

HF - High Frequency

VHF - Very High Frequency

LLS - Lightning Location System

LIS - Lightning Imagining Sensor

TRMM - Tropical Rainfall Measuring Mission

NASA - National Aeronautics and Space Administration

NOAA - National Oceanic and Atmospheric Administration

FOV - Field Of View

CCD - Charge Coupled Device

RRTP - Real Time Event Processor

LCFA - Lightning Cluster Filter Algorithm

NetCDF - Network Common Data Form

GOES-R - Geostationary Operational Environmental Satellites - R Series

LAN - Local Area Network

Chapter 1

Introduction

1.1 Objective

This Bachelor Final Thesis presents a characterization of both space-based optical Geostationary Lightning Mapper (GLM) detector on board the Geostationary Operational Environmental - R (GOES-R) series satellites and ground-based radio frequency sensors of Colombia Lightning Mapping Array (COL-LMA) installed in the tropics.

The present dissertation aims to introduce a new approach for the lightning detection, which takes advantage of the LMA located in the Colombian region of Barrancabermeja. Two methods based on spatio-temporal dimensions of rays derived from both GLM and LMA sensors are compared in order to analyze the sensitivity of the flash algorithm to changes in the grouping criteria, i.e. the distance between consecutive strokes and the duration of the flash.

1.2 Scope

In order to obtain much more information of the lightning activity, GLM and LMA signals will be compared using cross-correlation. This section outlines the key elements to proceed from study on the field to results outputting. In this way, this dissertation will include the following set of work packages that will allow the achievement of the proposed objective.

The theoretical framework and characterization of lightning detection will be devoted to provide a solid background of the thesis by focusing on the following elements:

1. An in-depth analysis of the theoretical framework regarding physics of lightning, with a particular focus on characteristics of lightning as a function of season location and storm type and conditions conductive to the occurrence of lightning.

2. An overview of the previous researches in this field of study and their contribution to the actual knowledge.

3. Non-exhaustive descriptions of the sensors involved in the space-based detection systems and in the current ground-based lightning spotting instruments.

Regarding on the numerical and computational part, a comparison on the exploration of the influence of the LMA sources' properties on its likelihood to be detected with GLM sensor assessments will be obtained through the following items:

1. The methodology followed for the analysis of GLM and LMA data sets.
2. Development of a general resolution algorithm capable of generating qualitative plots and able to compute power, height, number of events and more specific parameters of LMA sources not detected by GLM.
3. A brief characterization of the computational basis of the data processor and its main variations.
4. Analysis of the correlation between GLM and LMA data of high-energy lightning observed.
5. Comparison of space-based and ground-based detection systems via 3D mapping of the data obtained for both instruments.
6. Verification and validation of the results acquired for the two different lightning detector systems.

In summary, the main goal of this dissertation is the evaluation of lightning detections from space using high-resolution Lightning Mapping Array systems and as sub-goals, reviews of flashes and flash image generators and the development of codes for the evaluation of the data obtained.

Nevertheless, due to a shortage of time, the parameters compared during lightning performance will not be utilized in a rare-event logistic regression analysis to produce statistical models that predict the probability of the occurrence of lightning.

1.3 Requirements

This thesis will be developed in collaboration with the UPC Lightning Research Group, involved in different projects; aiming to optically resolve fast processes in lightning and sprites through detectors capable to detect energetic radiation from lightning. Focusing on obtaining 3D images of the performance of lightning over the LMA network, the following requirements are derived in order to study the mechanisms of lightning in the atmosphere.

1. Comparisons must be made independently of the different instruments' nature.
2. Data output must be equivalent among different instruments in order to be able to make a comparison.
3. The developed program and its functions should be based on free software for compatibility reasons.
4. Accuracy of results must be inside acceptable margins as to base a scientific study upon them.
5. Verification plots must be included in the report as to understand all processes and their accuracy.
6. Result plots must be included in the report as to show the final output of the program.
7. The program must check a minimum correlation among different instruments' data to better determine a match.
8. The program must be fully modular in order to make it comprehensive and easy to retouch.
9. The analysis must accept automatization of routines to study n cases without problems, regardless of the size of the input.
10. A full documentation of the code should be made in the report.
11. Code documentation must explain clearly every step of the script.

1.4 Justification

Lightning discharges in Earth's atmosphere are clearly among the most dramatic natural phenomena in human experience. It produces the brightest light and the loudest sound commonly occurring on our planet. The seemingly random occurrence of lightning in space and time, and the wide range of its significant temporal variations, from tens of nanoseconds for many individual processes to nearly a second for a full discharge and its eclipsing by the nascent thundercloud, make lightning particularly difficult to learn.

A detailed characterization of lightning activity for a specific region is required in a variety of fields; from meteorology and climatology to lightning risk assessment and protection design in a large number of disciplines, such as aeronautics. Moreover, lightning is an important source of high-energy radiation affecting atmospheric electricity, such as the propagation of radio waves. Quantifying the impact of lightning on the Earth system and understanding where and how lightning poses hazards requires an estimation of the timing, geographic distribution, and intensity of lightning strikes on a continental and global scale. Large-scale maps of the occurrence of lightning are as important to many models of land surface and atmospheric chemistry as temperature or precipitation maps, and are in themselves valuable for understanding various weather phenomena. Observing and mapping lightning distribution at large spatial scales has thus been a priority for the community for nearly a century.

To this end, the geolocation of lightning discharges, or particular physical processes within discharges, is important in a wide variety of applications. The most common way to geolocate lightning is by using a Lightning Locating System (LLS), which may be a ground-based or satellite-based electromagnetic (including optical) sensor or a network of sensors. Total lightning detection, defined as the combination of cloud-to-cloud and cloud-to-ground lightning, is limited to the use of these type of instruments and networks. In this study, GLM and LMA sensors performance is compared, as the validation of these lightning detection systems performance characteristics, such as detection efficiency and location accuracy, provides critical information about the behavior of the Earth's atmosphere. This would allow for better future analysis and results in lightning detection studies as well as for better tuning in future detection systems.

Chapter 2

Background

Since the dawn of time, lightning has been an incredulous natural phenomena present on Earth. Dangerous, uncapturable and fleeting, it has always intrigued humans. Although for many years, this natural occurrence has been largely inexplicable, recent breakthroughs in technology have given effective ways of understanding lightning. This chapter will further expand on the physics behind this tremendous event.

2.1 Electrical Characteristics of the Atmosphere

The principal components of air in the Earth's atmosphere are nitrogen (78%), oxygen (20%), noble gases (1%), water vapour (0.03%), carbon dioxide (0.97%) and other trace gas species. In general, air is a good insulator, due to the presence of a relatively small number of charged ions that can maintain its insulating properties until the applied electric field exceeds a critical value at standard atmospheric conditions that is about 2.8×10^4 V/cm [1]. Due to the ionization of the air in the lower ionosphere by the high-energy rays, cosmic rays and radioactive gases generated by the Earth, one cubic centimeter of air near the surface contains about 10 free electrons. When the electric field exceeds the above critical value, the air is immediately converted into a conductive medium and the current can flow in the form of sparks. The threshold electric field required for the electrical breakdown of air is a function of atmospheric density [1].

$$E = E_0 \frac{\delta}{\delta_0} \tag{2.1}$$

where δ_0 is the density of air at sea level at standard atmospheric conditions and E_0 is the corresponding critical electric field necessary for electrical breakdown under the same conditions [1]. Since the density of air in the Earth's atmosphere decreases with height with $\lambda_e = 7.64 \times 10^3$ [1], the critical electric field necessary to cause electrical breakdown in the atmosphere decreases with height as [1]

$$E = E_0 e^{\frac{-z}{\lambda_e}} \tag{2.2}$$

When the electric field in the atmosphere rises above this critical value, the resulting critical discharge generation depends on the spatial fluctuations of the pressure and the Earth's electric field [1]. The result is both potential differences and temperature changes between the lower and upper atmospheres, forming storm clouds [1].

2.1.1 Global Electric Circuit

Atmospheric electricity plays a variety of roles in the strongly coupled system that makes up the Earth's atmosphere and the space environment close to Earth. It has been known for more than two centuries that the solid and liquid Earth and its atmosphere are almost permanently charged. There is a net negative charge on the surface, and the opposite positive charge is equally distributed throughout the atmosphere. The surface electric field in fine weather is usually 100 to 300 V/m [2]. However, there are many factors that cause daily, seasonal, and other temporal variations in the region.

The conductivity of the clear atmosphere near the surface is on the order of 10^{14} mho/m [2] and increases almost exponentially up to an altitude of 60 km and at an altitude scale of 7 km. The main charge carriers less than about 60 km are small positive and negative ions produced primarily by Galactic Cosmic Rays (GCR). Beyond 60 km, free electrons become more important as charge carriers, and their high mobility causes a sharp increase in the conductivity of the entire mesosphere. Beyond 80 km, the geomagnetism causes the conductivity to become anisotropic and diurnal due to the Sun's photoionization process [2].

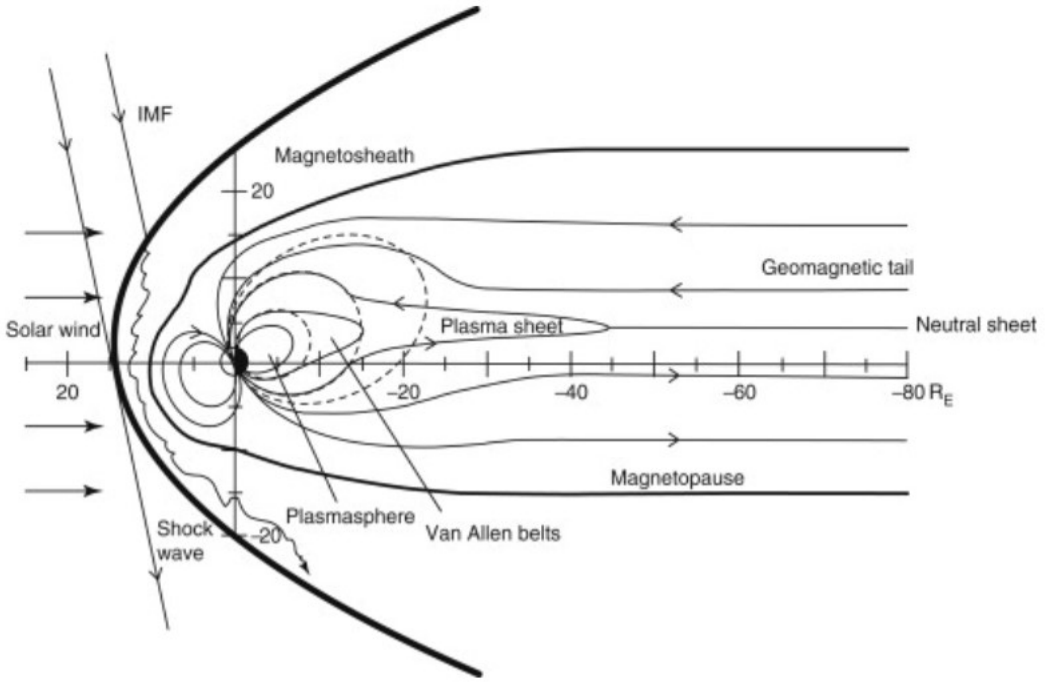

Figure 2.1: A sketch of Earth's magnetosphere in the noon–midnight plane. Extracted from [2]

As it can be seen, Figure 2.1 represents the Earth's layers in the noon-midnight plane. The dashed lines are the original dipole field. The solid lines are magnetic fields modified by external currents and IMF stands for interplanetary magnetic field, which is of solar origin. The area for the subject of atmospheric electricity is the electrically insulating concentric layer between the highly conducting Earth and the highly conducting ionosphere [2].

According to the classic figure of atmospheric electricity, all thunderstorms that work together charge the ionosphere to a potential of hundreds of thousands of volts compared to the surface of the Earth. This potential difference drives the electrical conduction current in the vertical direction from the ionosphere to the ground in all fair-weather regions

of the globe. The wire current in fair-weather depends on the potential difference of the ionosphere and the column resistance between the ionosphere and the ground. Horizontal currents flow freely in the ionosphere along the Earth's highly conductive surface. Current flows from the cloud top of the storm to the ionosphere and from the ground to the storm generator, completing the circuit as shown at Figure 2.2. The global fair-weather load resistance is 200 Ω [3].

The theoretical foundations of the subject of atmospheric electricity are firm, being based on the laws of physics: The Navier-Stokes and continuity equations and the laws of thermodynamics, which are required to understand and predict atmospheric motions. The atmospheric density decreases exponentially with increasing height, with a scale height, $H \sim 7$ km [3]. The atmospheric conductivity σ increases with height due to the energy spectrum of cosmic rays and the charged particles precipitating from the magnetosphere. By Ohm's law which is valid for linear processes only [3]

$$J = \sigma E \tag{2.3}$$

where J is the vertical electric current density and E is the vertical electric field [3]. This leads to expect that in order to maintain current continuity, E is largest near the Earth's surface, where its value is, from observations, ~ 130 V/m [3]. It decreases upwards, exponentially. By Gauss' law, there is a space charge profile associated with this electric field.

Since it is difficult to obtain global measurements to infer the momentary characteristics of GEC, there are models that provide an approximate equivalent circuit that scales the current through the ionosphere from the Earth's surface grid thunderstorm generator.

With R_1 being the charging resistor, R_2 the resistance of the thunderstorm generator where there exist potential differences ~ 100 MV [3] between the positively charged top of the thundercloud and the negatively charged bottom and R_3 the resistance of the boundary layer of the atmosphere, all of which are much greater than r, the resistance of the fair-weather atmosphere, it follows that

$$I = \frac{R_2 I_0}{R_1 + R_2 + R_3} \quad \longrightarrow \quad I \sim 1250\ A \tag{2.4}$$

Regarding these relations, the simple equivalent circuit shown in Figure 2.2 is considered [3].

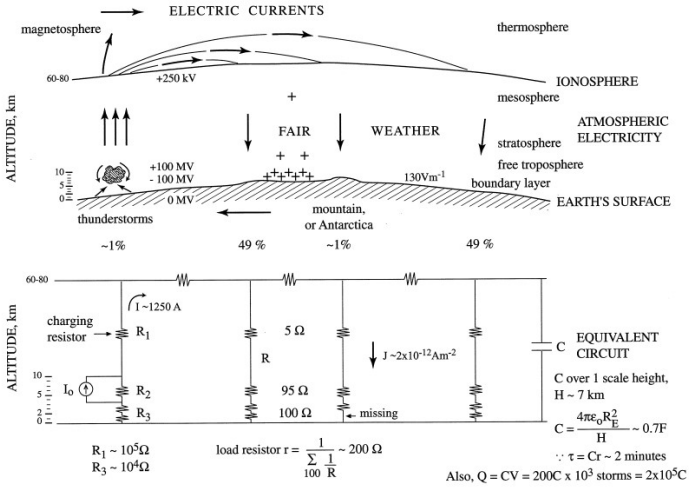

Figure 2.2: Diagram of the Global Electric Circuit. Extracted from [3]

Equation 2.4 relates the current through the fair-weather atmosphere, I, to the current in the thunderstorm generator, I_0. Measurements of I at a high altitude observatory, remote from active thunderstorms can give some information on I_0 if R_1 and R_2 can be considered to be constant [3]. However, increasing the flux of energetically charged particles associated with increased geomagnetic activity can reduce both. The figure 2.2 shows the currents flowing through different parts of the atmosphere, including the magnetosphere above. The lower part of the figure shows an equivalent circuit with three different regions. One of these is for high altitude part of the Earth where the profiles of J and E through the fair weather atmosphere will differ from those elsewhere.

From standard electrostatic theory, the capacitance C of the concentric layer of atmosphere between the Earth and the ionosphere, over one scale height of atmosphere rather than over the full height of the ionosphere, is given, taking into account that $H \sim 7$ km [3], by

$$C = \frac{4\pi\epsilon_0 R_E^2}{H} \quad \longrightarrow \quad C \sim 0.7\ F \tag{2.5}$$

where R_E is the radius of the Earth and ϵ_0 the permittivity of free space [3].

Hence the time constant for the atmospheric Global Electric Circuit, τ, is given by

$$\tau = Cr \quad \longrightarrow \quad \tau \sim 2\ min \tag{2.6}$$

With a charge of 200 C associated with each thunderstorm, the total Q on the plates of the spherical condenser is $2 \cdot 10^5$ C. Thus, the energy associated with the GEC circuit, considering $V = 250$ kV, is enormous; and it is [3]

$$Q = \frac{CV^2}{2 \sim 2 \cdot 10^{10}\ J} \tag{2.7}$$

The electric current density through the fair-weather atmosphere, J, has the $\sim 2 \cdot 10^{-12}$ A/m^2. Taking the conductivity of air at ground level, produced by extremely energetic cosmic rays and by radon from the ground and due to aerosols, to be $\sim 2 \cdot 10^{-14}$ mho/m, the fair weather vertical electric field at ground level is ∼100 V/m, close to the near observed value of 130 V/m [3].

Maxwell's equations are included to explain the electromechanical or electromagnetic effects rather than electrostatic phenomena. These equations relate the electromagnetic field to the charge and current densities in situations that change over time. It can generate and propagate electromagnetic waves of appropriate frequency. The flowing medium is equal to the square root of the relative permittivity. The medium is treated as a conductor at frequencies such that $\omega \ll \sigma/\epsilon_0$. Alternatively, the medium behaves as a leaky dielectric when $\omega \gg \sigma/\epsilon_0$; that is the situation in the ionosphere for VHF waves for higher frequency waves. Radiation produced by the current pulse due to cloud-to-cloud lightning discharge ranges resonance frequencies up to ∼100 MHz [3].

Nevertheless, if the radiation effect is not taken into account, the current flowing through is the sum of the line current and the displacement current. This is called Maxwell current. Other important contributions to current density can occur in the atmosphere due to convection, turbulence, precipitation (or sedimentation), or point discharge [3].

2.1.2 Thunderclouds Electrification: Formation and Dynamics

The conductivity structure of the giant spherical condenser and electromagnetic waveguide is determined by the interaction of ionization from the Sun and space with an exponential decrease in air density due to height above the Earth's surface [4]. In treating the DC Global Earth Circuit (GEC), the current source is basically a mechanism that vertically separates positive and negative charges between the conductive ground and the upper atmosphere. These mechanisms are due to microphysical processes including vertical charge transport at the planetary boundary, gravity-driven descent of selected aerosol particles in the atmosphere, and thunderstorm ice, which are the main sources of electric fields and currents in the Global Earth Circuit, as the current output from the thunderstorms around the globe maintains a vertical potential difference between the ground and the ionosphere [2] [4].

Therefore, thunderstorms are the result of thermodynamic, microphysical, and electrical processes. Strong vertical air currents and storm clouds are the result of excessive heat and humidity at low altitudes. In a global sense, this stratification of properties results primarily from the radiative properties of atmospheric constituents. The atmosphere is almost transparent to solar radiation, which is concentrated in the yellow part of the spectrum. Most of the solar energy that is not reflected by clouds passes through the atmosphere without being absorbed and is converted to heat on the ground or in oceans. The absorbing surfaces also radiates, but because its temperature is much lower than the Sun's terrestrial radiation is concentrated in infrared wavelengths. Atmospheric CO_2, water vapor, and other trace components in the atmosphere absorb much of the outward infrared radiation significantly, essentially blocking the outward radiation and further warming the air at low altitudes.

Average temperature at low altitudes guarantees long-term equality between heat dissipation and heat absorption [2]. Removal processes include some radiative losses through spectral windows between absorbing bands of CO_2 and water vapour and transport of heat by air parcels in motion. This latter process is known as convection. The heat gained on the surface is highly transported by convection. At this altitude, the radiation process is more effective because there is less absorption medium at the top [2]. Figure 2.3 shows that, globally, thunderstorms are most frequent in low altitudes near the tropics where a larger super-plus of heat is transported upwards by convection [4].

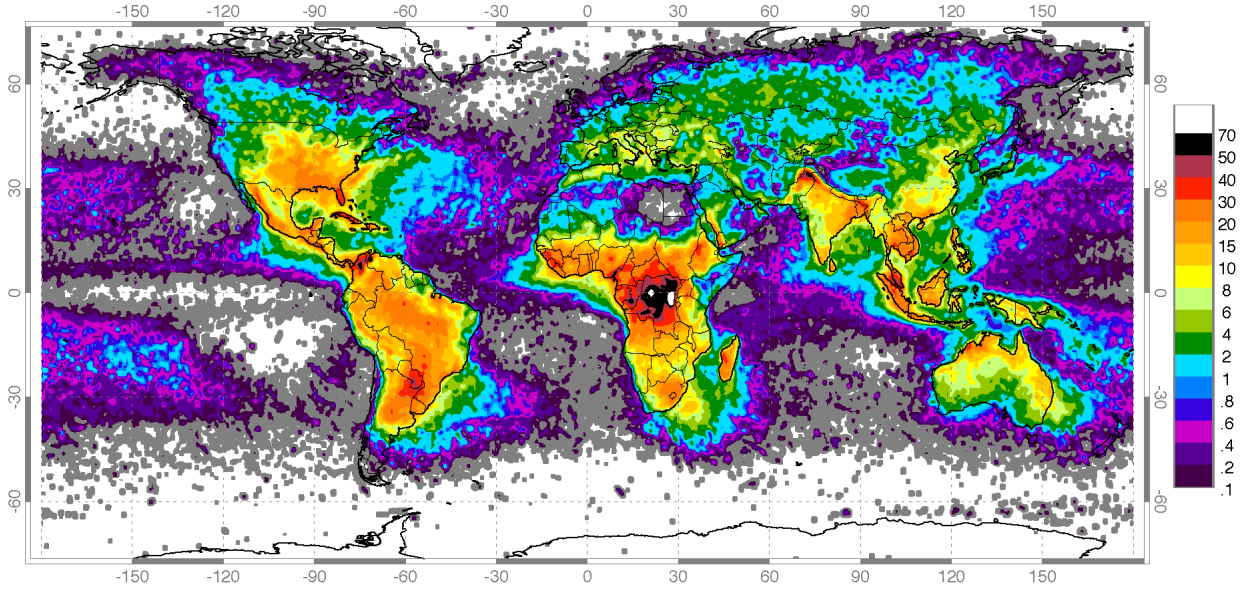

Figure 2.3: Global Distribution of Thunderstorms. Extracted from [4]

The process of vertical convection in the air mass is in contrast to the global process caused by very large horizontal temperature differences. Therefore, the equatorial zone is warmer than the polar regions and there are various circulation regimes that help reduce this temperature contrast. These predominantly horizontal circulations are also associated with vertical air movements, which tend to enhance and in some cases reduce favorable conditions for heavy thunderstorm vertical circulations [4].

About 85% of the atmospheric mass is contained in the lowest 13 km and this is the layer that generally participates in the vertical circulation of a typical thundercloud [2] [4]. Vertical air circulation during thunderstorms is due to differences in density. When the air is relatively warm, it inflates and is lighter than similar sized packages nearby. Warm packs are exposed to altitude-dependent compressive forces that depend on the weight of air in large environments and are not completely offset by the weight of the warm pack. Imbalance is represented by a net upward force (buoyancy). This raises warm packets that inflate in the face of a drop in air pressure. This expansion represents an environmental work done on the environment and is accompanied by a decrease in temperature. Ascending packets will continue to rise as long as they remain warmer than their surroundings. This means that the ambient temperature should drop with altitude at or above the same speed as the environment.

Thunderstorms only occur when the ambient temperature drops sufficiently with the height of the deep layers. If there is no moisture in the air, there are no thunderclouds. Therefore, the development of powerful convection systems creates extreme buoyancy that depends on stratified temperature, humidity, and horizontal wind and tends to accelerate the movement of both rising and falling air particles.

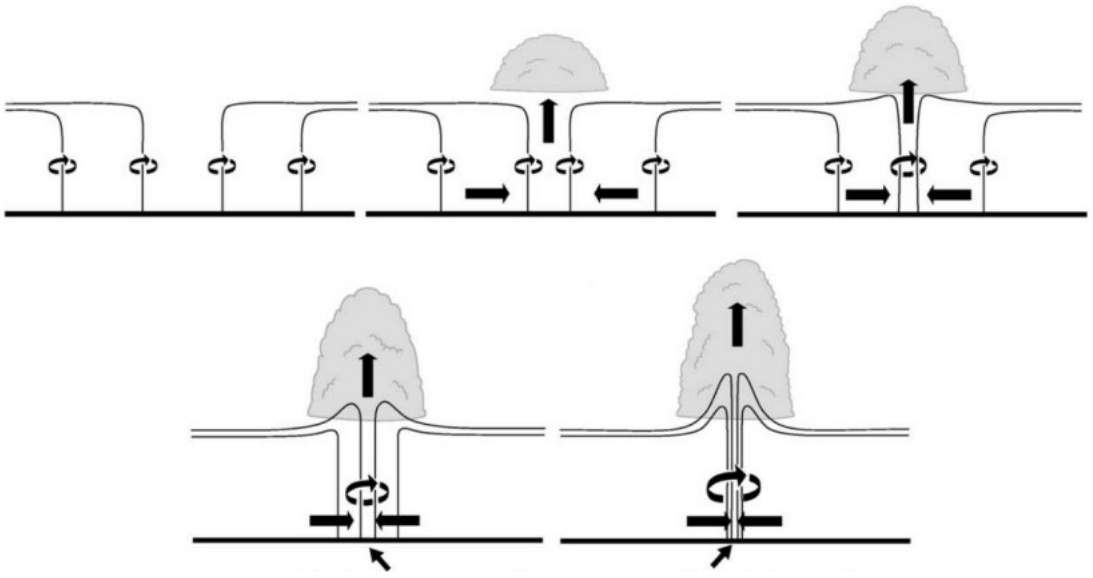

Figure 2.4: Thundercloud Formation. Extracted from [4]

Finally, thunderstorm electrification requires an understanding of the dynamics, microphysical and electrical properties of storm clouds, as well as their dynamics and precipitation processes [2].

The distribution and movement of charges in and around thunderstorms is complex and changes continuously as the thunderstorm progresses. Inside the storm is a dipole charge distribution consisting of a positive charge above the cloud and a negative charge below the positive. These are the dominant charge accumulations in the storm, called the

upper positive and main negative charges at the top, respectively. The positive charge at the top draws negative ions from the clear conductive air around the storm to the cloud top. The ions generated by cosmic rays attach to small cloud particles at the edge of the cloud, forming a negative shielding layer that partially cancels or shields the internal positive charge from outside observers. The main negative charge causes a point discharge or corona of trees, vegetation or other sharp or exposed objects on the ground under the storm, leaving a positive charge on the air above the surface. Charges accumulate in the upper positive and almost negative regions as a result of the charging mechanism until electrical stress causes a flash discharge [4].

he charging mechanism provides a power source that continuously increases the electrical energy of the clouds, and lightning intermittently reduces the electrical energy of the storm. The charging current is on the order of 1 A and ranges from an infrared value of about 0.1 A in the early stages of a small storm to a value above 1 A in a complex of large storms [2]. Equivalent average magnitude flows between clouds and the ground, and between the upper atmosphere and cloud tops. Cloud top current results from the flow of negative shield charge to the cloud top. The current between the clouds and the earth is generated by the action of lightning and point discharges from the surface of the Earth. This transfer, from approximately 1000 storms [2] [4] that are estimated to be in progress at any time over the entire planet, is thought to be the reason that the ionosphere is maintained at a potential of several hundred thousand volts with respect to the Earth's surface, as mentioned in the Global Earth Circuit.

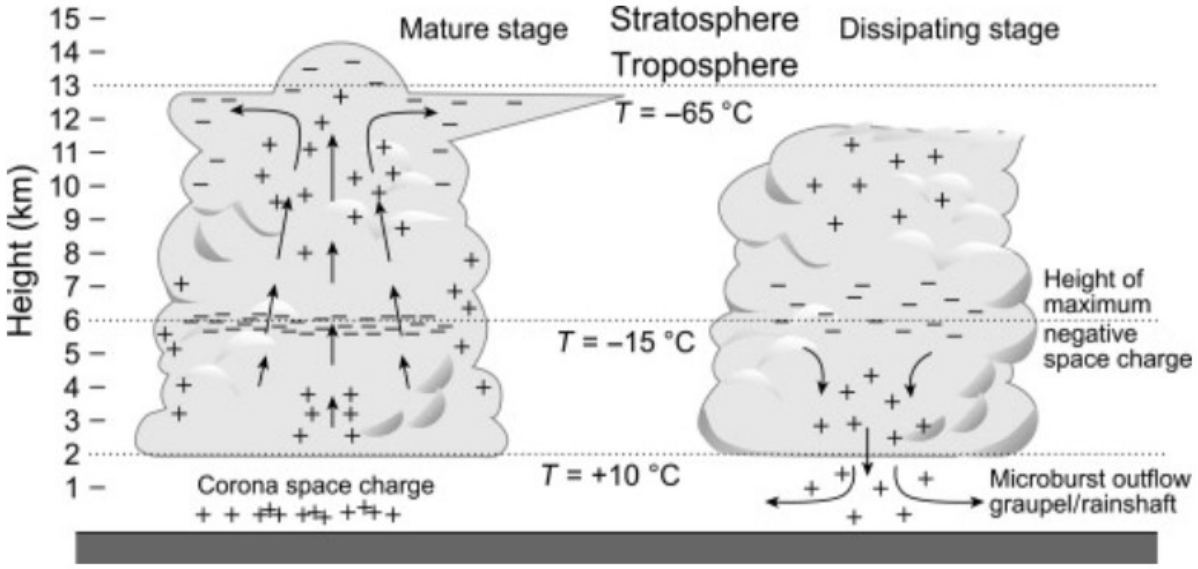

Figure 2.5: Electric currents for convection scenarios of electrification. Extracted from [4]

Most of the charge in a storm is in clouds or precipitation particles. Free charges or ions, such as those produced by cosmic rays, corona, or lightning, collide with cloud particles and attach to them within about a second of their formation. This fixes the charge and makes the cloud a good electrical insulator. The current that charges the storm should not be significantly dampened by the leakage current between the charging regions, except with the movement of charged cloud particles that are expected to have little effect. Therefore, the storm charge and electric field are expected to accumulate in a way that reflects the intensity of the charging process until a lightning strike, after which the accumulation is repeated [2] [4].

2.1.3 Discharge Processes

The physical processes that take place during the formation of an electric discharge can be characterized as follows. The electrical breakdown in a gas starts with a single electron which will lead to an avalanche of electrons created through the electron collision ionisation. As the avalanches grows the electric field starts to modify the electric field in the vicinity value the avalanche will convert itself to a streamer discharge. The heat generated by the streamer currents will increase the temperature of the streamer stem that when it reaches a critical value the conductivity of the stem increases and it will convert itself to a leader discharge.

Electron Avalanche

An electron avalanche is an exponential growth of electrons [5]. This growth is due to an increase in the background electric field above the critical value required for cumulative ionization. In this situation, an electron can generate other electrons through the generated ionization collisions.

As can be seen in the following equation, where α is the number of collisions per unit length caused by the electron moving in the direction of the electric field, and ν is the number of attachments that are the same length; the number of electrons increases exponentially as the distance from the initial conditions increases [5].

$$n_x = e^{(\alpha-\nu)x} \tag{2.8}$$

It is important to note, that the value of n_x is subject to variations due to the statistical nature of the collision processes [5]. Figure 2.6 shows a photograph of this event.

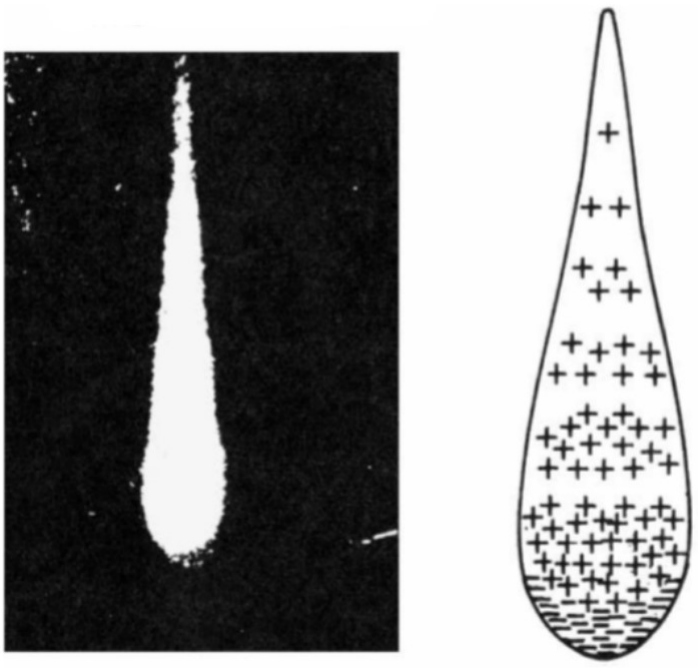

Figure 2.6: Single electron avalanche. Extracted from [5]

Assuming that these electrons of the avalanche are confined to a spherical region of radius r, then the electric field of the avalanche is given by

$$E_r = \frac{ee^{\alpha x}}{4\pi\epsilon_0 r^2} \tag{2.9}$$

where e is the electronic charge. Moreover, considering the diffusion made by the random electrons, the average radial distance of diffusion can be calculated from $r = \sqrt{4Dt} = \sqrt{\frac{v_d}{4Dx}}$, where t is the time of advance of the avalanche, D is the coefficient of diffusion and v_d is the drift velocity of the electrons [5]. Substituting this into Equation 2.9

$$E_r = \frac{ee^{\alpha x}}{4\pi\epsilon_0}\left(\frac{v_d}{4Dx}\right) \tag{2.10}$$

This equation shows that as the length of the avalanche increases, the electric field generated by the space charge increases, and the electric field generated at a particular critical length becomes comparable to the background electric field.

Streamer Discharge

As the electron avalanche spreads towards the anode. Weakly mobile positive space charge accumulates at the head of the avalanche. When the avalanche reaches the anode, the electrons will be absorbed, leaving a net positive space charge. Due to the recombination of cations and electrons, the avalanche head is a powerful source of high-energy photons. These photons create an additional avalanche near the positive space charge. When the number of ions in the avalanche head exceeds the critical value, the electric field generated by the space charge is comparable to the background electric field, and the secondary avalanche generated by the photons is attracted to the positive space charge. Secondary avalanche electrons are neutralized by the positive space charge of the cathode. This process is repeated, with the positive space charge head subsequently moving to the cathode [5].

This discharge is called a cathode direct streamer or positive streamer [5] and its formation process can be seen in the following Figure 2.7.

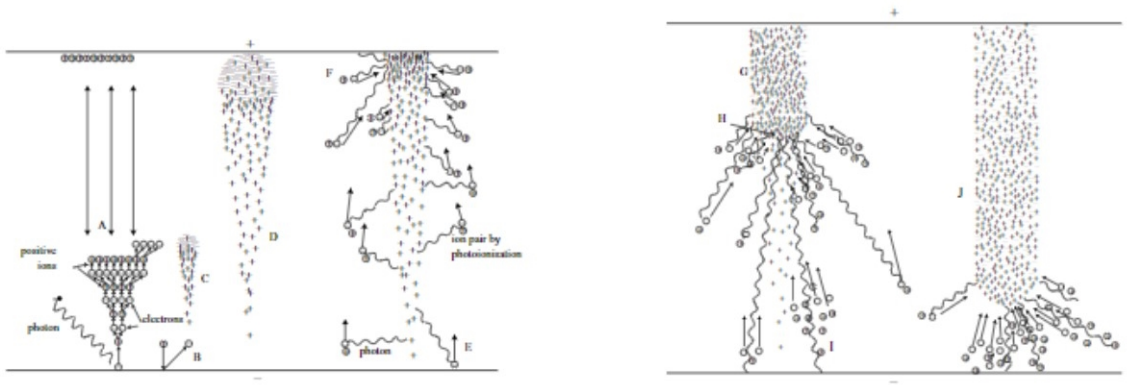

Figure 2.7: Positive streamer discharge formation process. Extracted from [5]

The formation of a negative streamer or an anode directed streamer is shown in Figure 2.8.

The avalanche electrons move to the gap, leaving a positive charge near the cathode. When the avalanche reaches the critical size, the secondary avalanche extends a positive space charge towards the cathode. When the positive channel reaches the cathode, both the increase in electric field associated with the proximity of the positive space charge to the cathode and the collision of positive ions at the cathode lead to the emission of electrons from the cathode. These electrons neutralize the positive space charge and create a weakly conductive channel that connects the negative head of the electron avalanche to the cathode. The high electric field of the avalanche head pushes the negative space charge further into the gap, and the remaining positive space charge is neutralized by the electrons supplied by the cathode and travels through the streamer head and cathode along the weak conduction channel. If the background electric field is very high, the positive space charge of the avalanche can reach the critical size required for streamer formation before reaching the anode. This can lead to the formation of a bidirectional discharge, both ends of which move to the anode and cathode, the former as a negative streamer and the latter as a positive streamer [5].

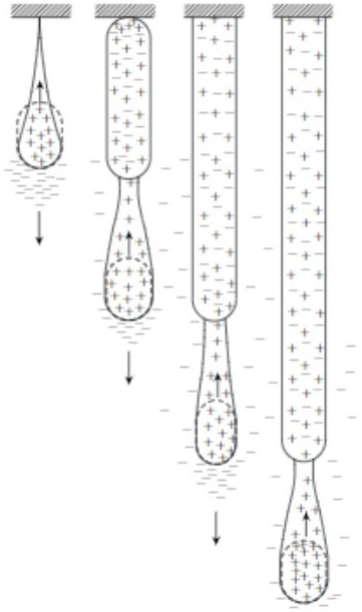

Figure 2.8: Negative streamer formation. Extracted from [5]

Corona Discharge

In many situations the electric field in air near objects at higher voltages or exposed to high external electric fields, can overwhelm the critical electric field required to form an avalanche. In addition, the range of volume in which this high electric field exists can be limited to a very small area around the object so that there is no breakdown between the object and the object in the vicinity. In this case, electrical activity is concentrated and limited to a small volume around the object. These types of discharge activity are called corona discharges [5]. In the case of corona discharge, ion space charges of both polarities accumulate near the high stress electrodes and change the electric field distribution. The balance between the accumulation and removal of space charge causes several types of corona discharge [5]. In addition, the physical properties of these corona discharges are affected by the electronegativity of the gas under consideration. Corona discharge has two different corona modes: negative corona mode and positive corona mode [5].

In the case of a negative corona, the electron avalanche begins at the cathode and develops towards the anode as the electric field diminishes. Due to their high mobility, electrons move rapidly from near the cathode to the low field region, leaving a positive space charge near the cathode. The electron avalanche stops at the surface where the electric field is below the critical electric field required for ionization. Here, the electrons are quickly captured by the electronegative oxygen atom, producing a negative space charge. These two space charge regimes (one positive and the other negative) modify the composition of the electric field in the gap so that the electric field increases near the cathode and decreases near the anode. The influence of this space charge will lead to three form of negative corona modes: Trichel streamers [5], negative pulseless glow [5] and negative streamers [5].

In positive corona mode, the primary electron begins an avalanche and grows towards the anode within the volume of the gas [5]. In this case, the electric field is higher than the critical value required for dielectric breakdown. As the avalanche grows in the direction of the increasing electric field, the electron drift rate increases as the avalanche increases, reducing the possibility of adhesion to electron-negative gases and the formation of negative ions. The electrons that reach the anode have high kinetic energies that must be dissipated by ionization collisions, resulting in discharge activity on the surface of the anode. The incident avalanche and electric field activity at the anode leave a positive space charge in front of the anode. If the number density of the positive space charge within a volume of about 50 μm radius exceeds 10^8 ions the streamer inception criterion is satisfied and streamers that propagate towards the anode are generated [5].

Figures 2.9 and 2.10 show either negative corona modes and positive corona modes from experimental studies.

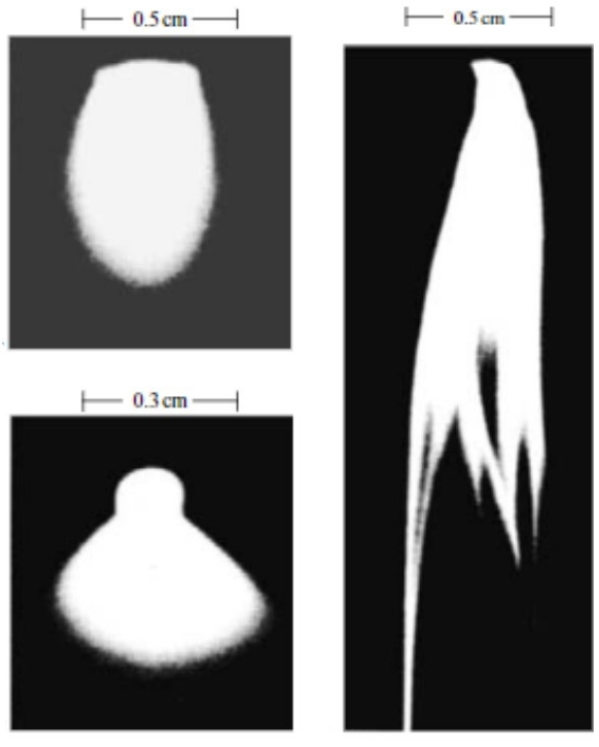

Figure 2.9: Different negative corona modes. Extracted from [5]

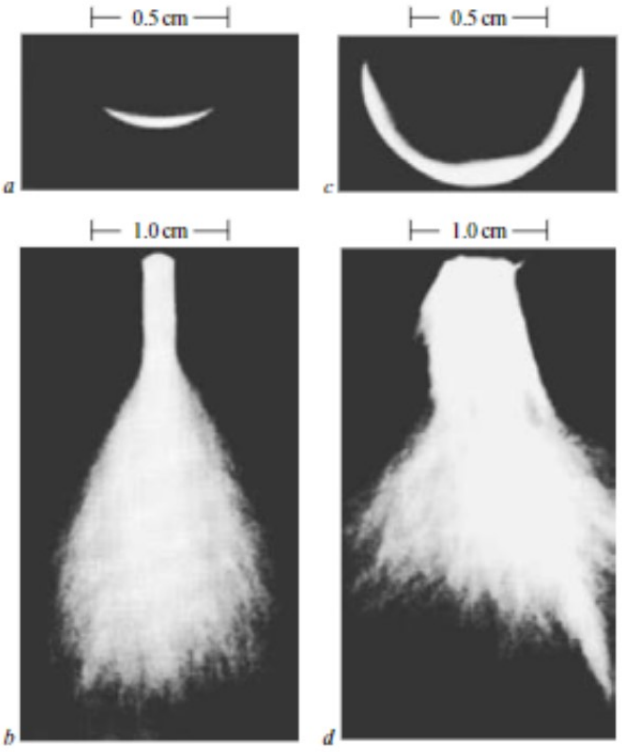

Figure 2.10: Different positive corona modes. Extracted from [5]

Leader Discharge

consists of a hot core surrounded by a cold, charged area called the corona envelope. The corona envelope is partly formed by the charge deposited by the streamer spreading in front of the leader channel and partly by the lateral corona discharge from the hot core [5].

Leaders appear to be moving forward in a series of rapid and discontinuous steps. The formation of steps can occur as a bidirectional discharge. When the negative charge flows forward towards the ground to create a new stage, the negative charge is removed from the top of the last read stage. The change in potential caused by the removal of the negative charge results in a positive charge that travels up the guide channel and transports the positive charge towards the cloud. This upward discharge manifests itself as a bright phenomenon spreading towards the clouds. When the bidirectional conductor is started, the negatively charged channel propagates downwards and the positively charged channel penetrates the center of the negative charge. The net charge of the guide channel is zero, since the negative charge is concentrated at the bottom and the positive charge is concentrated at the top. In this way, the leader is understood as a pillar of charge that extends down from the cloud. The potential gradient of the leader discharges is about 100 kV/m [5]. This is approximately equal to the background electric field necessary for the continuous propagation of a leader. This is also vindicated by the fact that lightning leaders travel to ground when the background electric field in air is in range of 60-100 kV/m [5].

The following figure is a representation of bidirectional stepped-leader formation.

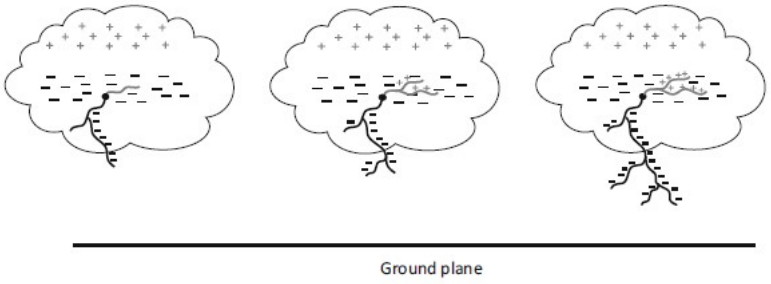

Figure 2.11: Bidirectional Stepped-Leader formation. Extracted from [5]

The front of the leader channel consists of a system of streamers, and when that streamer surface connects to either the ground or the streamer surface of the connecting leader that opposes it, setback begins. It can be assumed that the neutralization process starts at the confluence between the step ladder and the connecting ladder, one towards the ground and the other towards the clouds, in different directions [5].

2.2 Fundamentals of Lightning

Lightning is a temporary, high-current discharge that occurs in the atmosphere of the Earth and other planets, with a total path length on the order of kilometers. Most lightning is produced by thunderclouds, with more than half of all discharges occurring in the clouds [4]. The peak power and total energy of the flash is very large. So far, neither the geometric course of the lightning channel nor the full extent of lightning damage has been simulated in the laboratory. Lightning is a major cause of power and communication system failures and is also a major cause of interference in many types of cellular communications on advanced aircraft.

In addition to its many harmful effects, Blitz also has some unique advantages. Lightning is an important part of global electrical circuits because it plays an important role in maintaining charge on Earth. Therefore, it is clear that it is important to understand the physics of lightning in order to gain deeper insight into our geophysical environment and develop optimal protection against the danger of lightning.

2.2.1 Types of Lightning Flashes

A lightning flash is defined by the start of a conductor and multiple developments where the conductor can eventually reach the ground. The basic structure of a lightning bolt depends on which charged regions the lightning discharge occurs and which polarity transports the charge from one region to another. The two primary lightning flashes are Cloud-to-Ground [4] and Intra-Cloud lightning [4].

Cloud-to-Ground Lightning Flashes

Cloud-to-Ground (CG) lightning is a lightning discharge between a thundercloud and the ground [4]. This type of lightning always starts within the cloud with a process that is called the Preliminary Breakdown. The location of this process is not well understood, but it may begin in the high field region between the positive and negative charge regions from the electrified thundercloud. After several tens of milliseconds, the preliminary breakdown initiates an intermittent, highly branched discharge that propagates horizontally and downward stepped leader, where the negative charge are driven toward ground. When the tip of any branch of the stepped leader gets closer to the ground, the electric field just above the surface becomes very large and this causes one or more upward streamer discharges to begin at the ground and initiate the attachment process, as can be seen in Figure 2.12. The upward propagating discharges rise until one or more attach to the leader channel at a junction point that is usually a few tens of meters above the surface. Upon contact, the first return stroke begins. Recoil is essentially a powerful positive ionization wave that begins on or just above the ground and propagates through the guide channel at about one-third the speed of light. The peak currents in return strokes have typical values around 40 kA and these currents carry the ground potential upward and neutralize most of the leader channel and a portion of the cloud charge [4].

The last few steps of the stepped-leader, the onset of a connecting discharge and the beginning of a return stroke are illustrated in Figure 2.12 below.

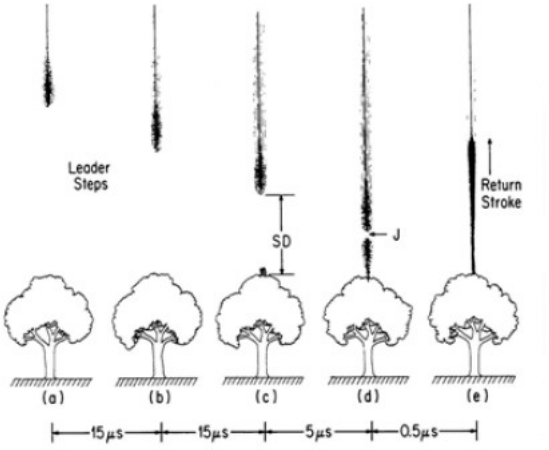

Figure 2.12: Attachment of a lightning stepped-leader to an object on the ground. Extracted from [5]

The parameters used to classify CG lightning are charge polarity, current magnitude, and lightning rod and flashback propagation direction [4]. Most CG flashes transfer negative charges from clouds to the ground, but there are flashes that transfer positive charges from clouds to the ground, called positive Cloud-to-Ground flashes. Positive lightning strikes tend to be much more intense than negative lightning strikes. Positive lightning produces both higher peak currents and longer lasting currents, allowing the surface to be heated to much higher levels [4].

Cloud-to-Cloud and Intra-Cloud Lightning Flashes

Lightning discharges also can occur between areas of cloud without contacting the ground. When it occurs between two separate clouds, it is known as Cloud-to-Cloud (CC) or inter-cloud lightning; when it occurs between areas of differing electric potential within a single cloud, it is known as Intra-Cloud (IC) lightning. IC lightning is the most frequently occurring type [2].

In response to the dipolar structure of the storm, the initial lightning discharges are usually intra-cloud flashes that transport charge vertically between the main negative and upper positive-charge regions. (IC) lightning is usually confined to the cloud interior and diffusely illuminates the cloud, being visible primarily at night. Intra-Cloud lightning often occurs as a primarily vertical discharge between the main negative and upper positive charge regions of the storm [2].

2.2.2 Mechanism of Lightning Flashes

Experimental remark of the optical and electromagnetic fields generated through lightning flashes have drastically superior our information regarding the mechanism of the lightning flash. The look at of atmospheric strength and, therefore, lightning research, has left at the back of descriptions of determined and measured lightning effects; capabilities and traits that preceded the expertise of lightning physics.

The key component of any lightning process is the leader, which is self-propagating discharge in an ambient electric field that produces a hot plasma channel with a continuing current [4]. The formation of leader discharge occurs during the transition of millions of cold corona rays that focus like sun rays through a magnifying glass to the tip of an electrode or the tip of an existing conductive leader. This process creates an element of the thermalized plasma channel in front of the chip and lengthens the leader channel.

The streamer-leader transition process that leads to elongation and, therefore, to the propagation of leaders is different for positive and negative leaders [4]. For positive leaders, positive corona streamers have a conical shape at the top of the conductor and their development is continuous. For negative leaders, the streamer-leader transition involves the formation of a piece of plasma called the space leader, shortly before the leader where the bidirectional corona occurs. The negative corona points to the outside and the positive corona points to the top of the main leader channel. The bidirectional formation of the corona from the space conductor leads to an arc discharge between the main conductor and the space conductor. This arc discharge creates an extension of the cascade conductor and is the main source of strong radiation in the VHF band [4]. Differences in the streamer leader migration process between positive and negative leaders are the main reason why negative leaders can be easily mapped using Lightning Mapping Systems, but positive leaders are rarely detected in these systems [4].

The start and progress of the leader depends on the formation of the corona streamer. The length of the corona streamer is determined by the ambient potential profile in front of the leader and the constant electric field maintained along the corona streamer [4]. Therefore, the potential gradient at the tip of the conductor promotes the development of the conductor after it is introduced. Propagation of the induction channel stops when the potential gradient at that peak falls below the threshold level required for breakdown to proceed before the peak [4]. When this happens, leader propagation stops and continuous flow within the leader stops. In this way, the entire flash process ends.

Bidirectional Propagation of a Leader

Once an electrical breakdown is initiated it gives rise to streamer discharges in turn give rise to a leader discharge. Once leader is created, it propagates in the background electric field, leading to either a cloud flash or ground flash [4].

The available propagation mode for the leader is to replicate itself as a bidirectional leader. When a neutral conductive channel is placed in a background electric field, charges of opposite polarity are concentrated across the conductive channel. This charge concentration increases the electric field at both ends, which causes a reverse-polarity streamer discharge from both ends of the conductive channel. When a streamer discharge of one polarity propagates forward, the charge of the opposite polarity accumulated in the conductor is utilized by the streamer discharge of the opposite polarity that moves from the other end. These streamer discharges increase the length of the leader channel by concentrating and conducting current on the streamer shaft [4]. Thus, the leader extends from both directions. The total charge on the leader remains zero while positive charges are concentrated on one end and negative charges on the other. This mode of propagation of the leader is called bidirectional leader propagation. All lightning leaders that originate in space without the advantage of a conducting grounded body propagate in this mode. The initiation of the leader may take place according to the mechanism described above. When started, the proto leader channel acts as a conductor placed in a uniform electric field, and if the background electric field is strong enough, the bidirectional propagation mode takes over [4].

Figure 2.13 shows the existing parts and determines the nature of either negative leader end and positive leader end

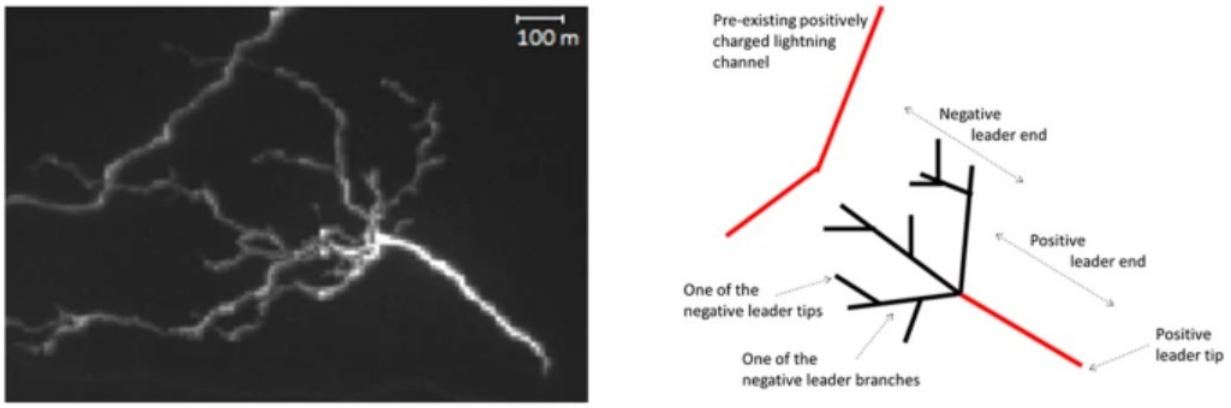

Figure 2.13: Bidirectional Leader Propagation. Extracted from [6]

Return Strokes

The connecting ladder can successfully fill the gap between the ground and the stepped leader that moves down. The object that started the successful connection guide is the object that was hit by a lightning strike. Once the connection between the stepped conductor and the Earth is established, a wave of ground-level potential travels along the leader channel towards the clouds, and the associated luminosity event moves upward at a velocity close to the speed of light in free space. This transmission event is called return stroke [4].

When a connection is made between the leader and the stepped leader, the potential of the first element of the stepped leader that the leader channel contacts changes from the cloud potential to the ground potential. As a result, the charge present in this channel element was needed to keep this element at cloud potential, but it is released and this charge flows to ground along the leader channel [4]. This also changes the potential of the next element on the leader channel that was adjacent to the grounded element and releases its charge. In this way, a wave of ground potential travels upwards, releasing a charge constrained by the cloud potential on the leader channel [4]. The released charge travels to ground along the stepped conductor channel. The flow of this charge to the ground creates a large current in the channel that shines brightly when heated. This high current region and the associated luminosity move up the channel as the charges present at higher levels along the stepped leader combine towards the ground with a dash. This process, in which the charge stored in the stepped conductor channel is conducted to ground, is called the return stroke [4].

The return stroke begins when the connecting leader penetrates the corona sheath of the stepped leader and then contacts the hot core of the stepped leader. First, the recoil propagates in two directions. One towards the ground and the other towards the clouds. As the return stroke passes through the stepped leader channel, the positive streamer becomes longer and the negative charge on the corona sheath is neutralized. This neutralization process rises, but the electrons emitted by the neutralization process generate a falling (negative) current [4].

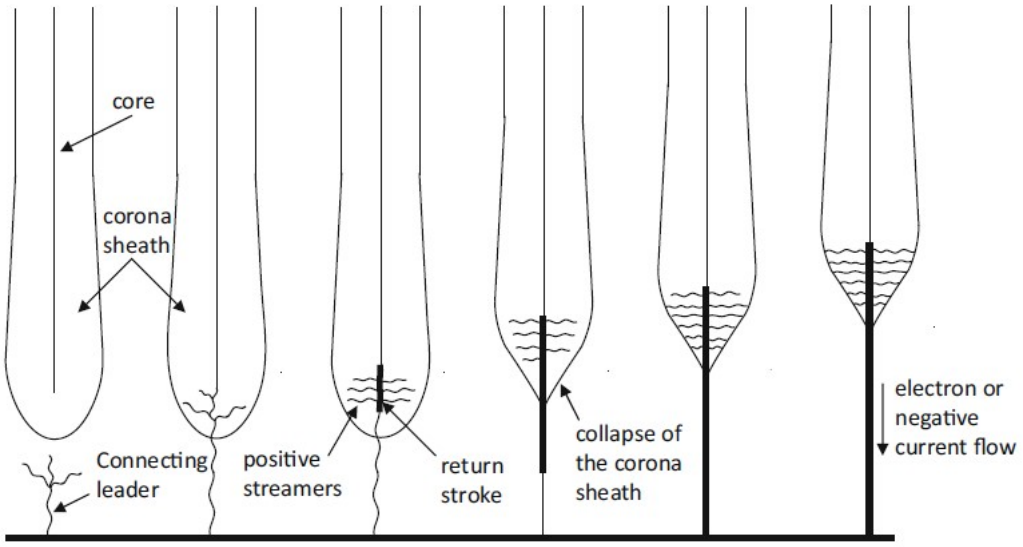

Figure 2.14: Return Stroke mechanism. Extracted from [4]

2.3 Lightning Flash Location Techniques

Lightning phenomenology includes the frequency of lightning observed on large spatial and temporal scales. This includes maximum and average lightning rates per unit area and changes in lightning characteristics depending on location and storm type [7]. Studies on lightning phenomenology can now be discussed in terms of both satellite-based and ground-based observations. The use of satellites is, mainly, for obtaining data of the incidence and distribution of lightning in the world related to continents and oceans. Extensive use of ground-based observations can be used to determine the incidence and characteristics of lightning in individual storms.

Lightning detection and locating systems can be divided into two categories. In detection systems that belong to the first category, the number of lightning flashes that strike a particular area is obtained without specific knowledge of the actual location of the lightning strikes. Flash counters fall into this category. Detection systems that can determine the detailed shape of the impact point or lightning channel fall into the second category. Examples include magnetic detection systems, arrival time systems, and radio interferometer systems [7].

2.3.1 Magnetic direction finding

In this technique, the direction of the horizontal component of the magnetic field generated by lightning is obtained at two spatially separated stations using intersecting magnetic loops [7]. Since the horizontal component of the magnetic field at a point is perpendicular to the direction of the lightning strike observed from that point, the information obtained from the two stations can be used in triangulation to determine the point of the lightning flash.

If the lightning channel is vertical and the signal received by the loop has no ionospheric reflections, the direction finder will provide the exact direction to the collision point. However, in general, the lightning channel is not vertical and the signal received by the direction finder may be due in part to the reflection of the magnetic field generated by the lightning from the ionosphere [7]. Both can cause errors in the direction finding system. The latest broadband magnetic direction detectors solve these errors using the first few microseconds of the backstroke signal without ionospheric reflections [7]. Also, the first few microseconds of the recoil signal are generated by the first few hundred meters of a nearly vertical, straight lightning channel.

A crossed-loop direction finder cannot determine if the signal received is due to a negative ground flash in one direction or a positive ground flash in the opposite direction. Ambiguity in this direction can be resolved by measuring the polarity of the electric field at the same time as the magnetic field and determining the polarity of the flash [7].

2.3.2 Time of Arrival Method in the VHF range

During the flash, the rise and duration are so short that it produces a large number of pulses that can excite a system tuned to the HF and VHF ranges [7]. When excited by an impulse a receiving system tuned to a central frequency f_0 and bandwidth B generates an oscillating output that decays in a time which is given approximately by $1/B$ [7]. If such an antenna system is used to tag the time of arrival of the impulsive events at several spatially separated stations the information can be utilised to obtain the location of the discharge events that gave rise to these impulses [7].

The dielectric breakdown process in the air produces pulses that can excite the VHF conditioning system and by mapping the location of the many pulses that generated such lightning, a three-dimensional image of the lightning can be obtained.

The VHF time of arrival systems can be divided into two categories, namely, Long Baseline Systems and Short Baseline Systems. In the long baseline systems the antennas are separated by distances of several kilometres. From the measured time of arrival of the same pulse at different stations hyperbolic geometry should be used to obtain the position [7]. In short baseline systems the incoming signal can be treated as a plane wave and straight line geometry can be applied. One difficulty with the long baseline systems is the difficulty of identifying the same pulse feature in different antennas. In addition, the number of impulsive events. Only a limited number of stations excite the receiver. Some of these issues can be avoided by using a short baseline system.

2.3.3 Radio Interferometric System

The general principles of VHF interferometry are as follows: Assuming a plane sine wave incident on two antennas, separated by a distance d and having a phase difference of ϕ in the output signals of the two antennas, it is related to the direction of arrival of the wave [7].

$$\phi = 2\pi d cos\left(\frac{\theta}{\lambda}\right) \tag{2.11}$$

where λ is the wavelength and θ is the angle between the direction of incidence of the wave and the line joining the two antennas [7]. Thus, by measuring the segment distinction of the output signal, the route of the incoming wave may be obtained. If the machine consists of 3 antennas, by measuring the segment distinction of the output of impartial pairs it is easy to estimate the azimuth and the elevation of the incoming plane wave [7].

Equation 2.11 shows that for a given angle θ the rate of change of ϕ with respect to θ is proportional to d/λ [7]. Thus, the higher this value, the more sensitive the measurement. However, for phase measurements, the distance between the two antennas or the baseline must meet the criteria $d/c \leq 1/B$ where c is the speed of light and B the bandwidth of the antenna system [7].

Chapter 3

Lightning Detection

Generally, for all applications of lightning data it is important to know the performance of the employed Lightning Location System (LLS). The performance characteristics of lightning location systems are determined by their ability to geolocate lightning discharges with high location accuracy, high detection efficiency and a low false detection rate and to report various other features of the lightning discharge correctly. Different methods or a combination of methods may be used to validate the performance characteristics of different types of lightning locating systems. In this chapter, GLM and LMA of both space-based and ground-based lightning detection systems are described and characterized in order to get information about performance variations over large spatial regions.

3.1 Space-based Lightning Detector

Space-based Lightning detectors enable new and unique views of lightning processes from cloud top that provide new scientific understanding and applications for lightning location features. Over the last decade, the maturation of satellite based observations of lightning has been marked by the successful operation of the Geostationary Lightning Mapper (GLM) on board the Geostationary Operational Environmental Satellites - R (GOES-R). This constellation of satellites were the first spaceborne platforms that observe lightning from a geostationary orbit and cover much of the Western Hemisphere. Compared with their predecessors working in Low Earth Orbits, the GLM aboard these geostationary satellites is able to provide more detailed information on the spatial propagation and discharge frequency of lightning with improved detection efficiency over its coverage.

The GLM is the first step in an international space-based observing constellation for continuous total lightning measurements on a global scale. Both the Low Earth Orbit satellites and geostationary satellites will host optical lightning imagers. The GLM builds on a legacy of optical lightning observations from low Earth orbit including the Lightning Imaging Sensor (LIS) on the Tropical Rainfall Measuring Mission (TRMM) satellite. The GLM results from decades of work toward detecting lightning from geostationary orbit.

3.1.1 Geostationary Lightning Mapper (GLM)

The Geostationary Lightning Mapper (GLM), conceptually, is a high speed event detector operating in the near infrared. It is designed to operate on the Geostationary Operational Environmental Satellite R-series (GOES-R) which becomes part of the original GOES constellation. This set of satellites deployed by the National Aeronautics and Space Administration (NASA) and the National Oceanic and Atmospheric Administration (NOAA) is responsible for providing weather forecasts and warnings. The aim of adding the GLM is to obtain greater accuracy in both timing and prediction.

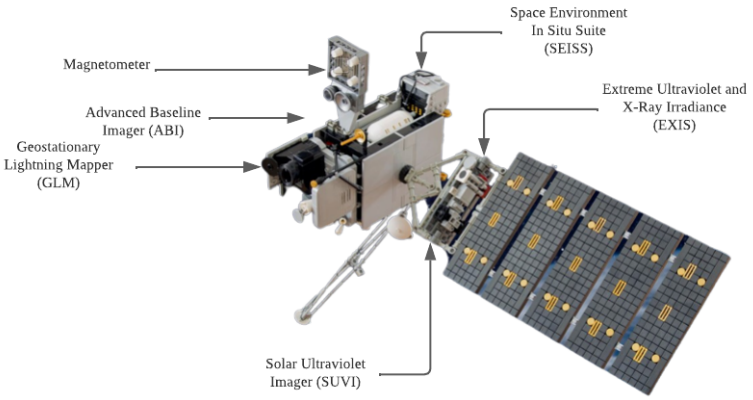

Figure 3.1: GLM location on board a GOES-R satellite. Extracted from [8]

The Geostationary Operational Environmental Satellites – R Series (GOES-R) is the constellation of satellites of interest in this thesis since the coverage area sweeps out the American continent where COL-LMA is also located. GOES-16, in operations as GOES East, keeps watch over most of North America, including the contiguous United States and Mexico, as well as Central and South America, the Caribbean, and the Atlantic Ocean to the west coast of Africa. GOES-17, which serves as GOES-West, watches over the western continental United States, Alaska, Hawaii, and the Pacific Ocean to New Zealand.

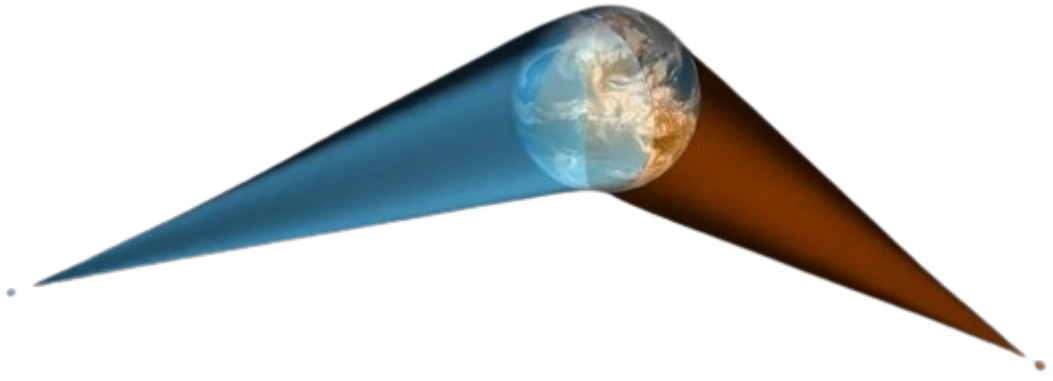

Figure 3.2: GOES-E and GOES-W coverage area. Extracted from [8]

Technologically, GLM is a 500 frame per second camera which its recollected data is distributed as pixel-level triggers above the bright cloud background and clustered through a three-level hierarchy into lightning flashes. GLM continuously monitors optical emission from both intra-cloud and cloud-to-ground flashes, across a near hemispheric coverage (18,000 km diagonal field-of-view) with a near-uniform round sample 8-14 km pixel footprint resolution, with the design requirement of detecting more than 70% of lightning flashes on a 24 hour basis.

Because of the transient nature of lightning, its spectral characteristics, and the difficulty of daytime detection of lightning against the brightly cloud background, actual data handling and processing is much different from that of a simple imager. A wide Field-of-View (FOV) lens combined with a narrow-band interference filter is focused on a high speed Charge Coupled Device (CCD) focal plane. Signals are read out in parallel from the focal plane into real-time event processors for event detection and data compression. The resulting event detections are formatted, queued, and sent to the satellite's Local Area Network (LAN).

GLM technical properties

The GLM performance characteristics are summarized in Table 3.1. The GLM is a Charge-Coupled Device (CCD) imager with a set of optical filters to detect lightning in a narrow 1 nm spectral band centered on 777.4 nm. The GLM consists of a single telescope with a variable pitch focal plane detector array of 1,72 $\times$ 1300 pixels. The array is divided into 56 subarrays for fast transient event processing by 56 Real-Time Event Processors (RTEPs). Each subarray is independently tuned to optimize the dynamic range and sensitivity, which vary based on the background scene. The variable pitch reduces the spatial growth of GLM pixel footprints away from nadir, so the pixel size only varies from 8 km at nadir to 14 km at the limb. The instrument relies on the spacecraft position and pointing information along with a coastline identification and navigation procedure to convert the focal plane x, y to latitude and longitude coordinates.

Table 3.1: GLM instruments specifications. Extracted from [8]

GLM instruments specifications	
CCD imager	1372 x 1300 pixels
Pixel FOV (nadir)	8 km
Pixel FOV (corner)	14 km
Wavelength	777.4 nm
Bandwidth	1 nm
Downlink Data Rate	7.7 mbps
Product Latency	$<$ 20 s
Operational Power	405 W

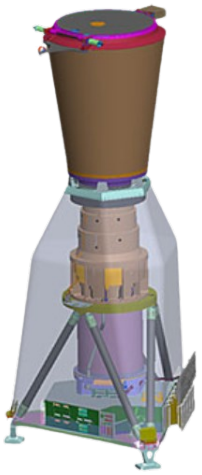

Figure 3.3: 3D model of GLM. Extracted from [8]

Data Categorization: Events, Groups and Flashes

A combination of lightning data sets are processed in the event processor incorporated into the Geostationary Lightning Mapper in order to geolocate this phenomenon. This data is organised by a three-tier of events, groups and flashes processed by the Lightning Cluster Filter Algorithm (LCFA), which integrates events into groups and groups into flashes.

- **Event:** An Event is the basic GLM data unit. It is defined as the occurrence of a single pixel exceeding the background threshold during a single frame; that is, each pixel output from the on-board instrument hardware and software produces a separate Event. Although an Event can be thought of as a single optical pulse from lightning, it is possible that multiple pulses occurring within the 2 ms frame may contribute to an Event or that a single lightning pulse may contribute to more than one Event.
- **Group:** The formal definition of a Group is one or more simultaneous Events that register in adjacent (neighboring or diagonal) pixels in the focal plane array. Groups do not always correspond to a single lightning pulse. A lightning pulse may be split across two Groups, or multiple lightning pulses may be contained in a single Group.
- **Flash:** A GLM Flash corresponds to several related Groups in a limited spatial and temporal range. A Flash may include as few as one Group with two Events (single Event Flashes are, for the most part, indistinguishable from noise, and so are currently removed from the GLM output by the LCFA), or it may consist of many Groups, each containing many Events.

Principles of operation

The GLM detector is a Charge-Coupled Device (CCD) pixel array and has a variable pixel pitch that keeps the ground sample distance of the pixels from exceeding 14 km over America. The GLM electronics monitor the background scene brightness detected by the CCD and on a frame-by-frame basis check for pixels that exceed a threshold that depends on the background. After filtering for shot noise, glint, radiation tracks, blooming due to stray light or glint, and other artifacts a detection is reported at each pixel exceeding that background in a single 2 ms frame.

In the case of lightning, a triggered detection usually corresponds to the pool of light emitted from the top of a cloud surface illuminated after the light from the lightning channel has scattered through the cloud. Groups that have any events within 16.5 km and 330 ms in weighted Euclidean distance are clustered into GLM flashes, encompassing the flickering light output expected to be produced by a connected lightning channel discharge tree.

The variable optical energy across each group and its spatial extent are the primary physical measurement quantities and are referred to as a lightning detection data set.

3.2 Ground-based Lightning Detector

The geolocation of lightning discharges, or particular physical processes within discharges, can also be done by ground-based lightning detectors. A ground-based LLS is typically a network of a minimum of four to five sensors and a central processor. Each sensor measures the electromagnetic signal produced by a lightning discharge and sends back information about the associated waveform characteristics to the central processor. Once a specific lightning event is measured by multiple sensors in a network and reported to the central processor, one or more techniques can be used at the central processor to geolocate the lightning event. Ground-based lightning location systems are able to determine the location, intensity, the type of lightning, track the movement of thunderstorm cells and the evolution of their charge structure in real time.

Over the last decade, the maturation of ground based observations of, specially, cloud-to-ground discharges has been marked by the successful operation of the technology implemented on Lightning Mapping Array (LMA) systems. Although this set of systems evidently contributes to the understanding of lightning phenomena, their implementation is currently concentrated in mid and high altitudes. Little research using LMA systems is being carried out in tropical regions where, paradoxically, the greatest lightning activity on the planet is concentrated. The Colombia Lightning Mapping Array (COL-LMA) results from the information gap on the tropical zone of Colombia and is able to characterize lightning leader processes by reconstructing trajectories, identifying the emission heights, propagation speeds and the polarity.

3.2.1 Colombia Lightning Mapping Array (COL-LMA)

Despite the fact that highest rates of global lightning activity occur in the equatorial region, electrical parameters within tropical thunderstorms are still not widely characterized. Nevertheless, the UPC provided in a specific Colombian region a 3-D Lightning Mapping Array (LMA) that reveals data of different lightning processes.

The LMA system detects radio emission sources in the very high frequency (VHF) range emitted by the electrical breakdown process of lightning channels and employs the time-of-arrival method to locate them three- dimensionally. The maximum magnitude of the VHF source power radiation is recorded every 80 μs and its time is synchronized according to a GPS-derived precise time. Each source requires detection by at least five stations to be located with an accuracy of about 50 and 100 m in the horizontal and vertical plane, respectively. Typically, a few hundred up to a thousand or more sources are located per lightning flash.

The Colombia-Lightning Mapping Array (COL-LMA) was first composed of six VHF receivers, in frequency ranges between 60 to 66 MHz, with baselines between 8 and 18 km distributed around the Colombian city of Santa Marta. In mid 2018, it is decided to augment with 2 more stations and relocate the COL-LMA network to one of the most active lightning activity sites in Colombia, the middle Magdalena valley, whose lightning to ground GFD density is estimated to be between 30-40 lightning strikes km^2/year. This region is located in central-western Colombia around the city of Barrancabermeja.

Geographical location of the Colombia-LMA network can be seen in Figure 3.4. Each triangle represents an LMA receiver around Barrancabermeja city. The high-efficiency coverage area is approximated by a buffer of 65 km.

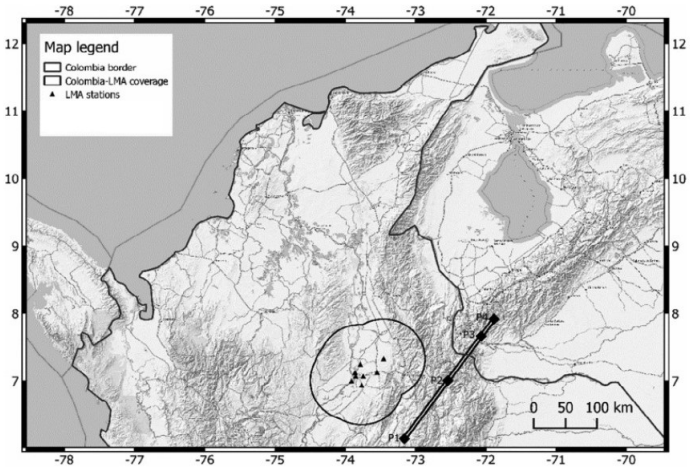

Figure 3.4: Geographical location of Colombia Lightning Mapping Array. Extracted from [9]

Principles of operation

Each station consists of a set of ground plate omnidirectional radio antennas tuned for a 6 MHz bandwidth between 60-66 MHz. The system has a 20 dB signal amplification stage, two band pass filter stages at the antenna output and at the input of the data acquisition system. At the software level, the stations record every 80 μs the peak value of emissions exceeding the allowed threshold with their respective absolute time via GPS. The temporal resolution of the system acquisition is 50 ns using a 20 MHz digitizer. Using the Time Of Arrival technique, the LMA can three-dimensionally reconstruct an electrical discharge up to a maximum of 10000 sources per second with RMS errors of vertical and horizontal location of approximately 100 and 50 meters respectively. At the operational level, each station has an auxiliary power system with batteries and communication via modem for remote management.

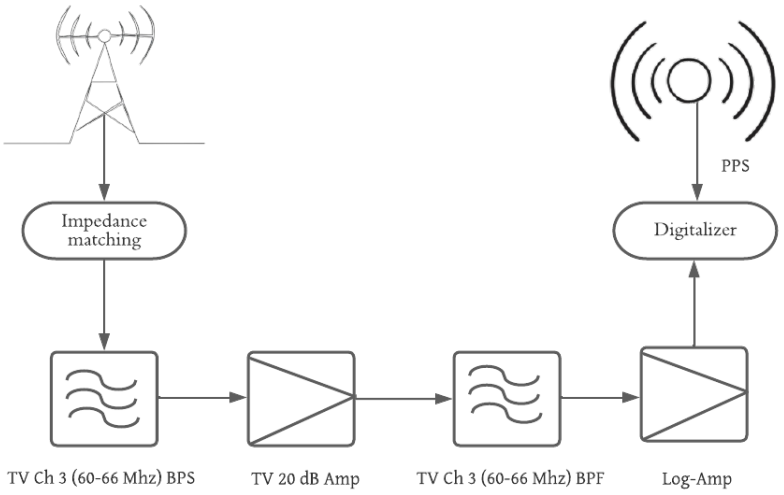

Figure 3.5: Simplified diagram and key components of the LMA system.

Chapter 4

Data Management and Methodology

In this chapter, the combined Geostationary Lightning Mapper (GLM) and Colombia Lightning Array (COL-LMA) data generated will be rated and processed in both lightning sensors in order to generate a model for predicting the mean source characteristics associated with each lightning location systems. The objective of this chapter is to give an introduction to the reader regarding what data formats and programs have been used to get the results displayed further in this document. Technical description of the codes nor the data will not be presented, but it should be regarded more as a comprehensive description of the intended algorithm.

4.1 GLM data

The GLM electronics monitor the background scene brightness detected by the CCD and on a frame-by-frame basis check for pixels that exceed a threshold that depends on the background. In the GLM data set, the triggered pixels are known as events, and the adjacent, triggered pixels in a single frame form groups. In the case of lightning, a triggered detection usually corresponds to the pool of light emitted from the top of a cloud surface illuminated after the light from the lightning channel has scattered through the cloud. Groups that have any events within 16.5 km and 330 ms in weighted Euclidean distance are clustered into GLM flashes, encompassing the flickering light output expected to be produced by a connected lightning channel discharge tree.

GLM data is extracted from the National Oceanic and Atmospheric Administration (NOAA) via a Google Platform Repository, where thousands of *.nc* files are stored with GLM information. Each register of 200 ms is ordered by year, day of the year and hour of the day. The Network Common Data Form (NetCDF), which gives the *.nc* files, is a vastly used platform open-source binary file format to share large amounts of array-oriented data in a way that is self describing, portable and efficient. These type of files contain information of the events, groups and flashes as well as the positioning and configuration of the satellite at every moment.

In order to extract only the information required for location and identification of lightning, a python code has been developed by UPC's Lightning Research Group. This program takes all the GLM data files saved in a specified folder and returns a *.txt* file with time, group latitude and longitude, flash ID, flash latitude and longitude, and energy for each event.

Figure 4.1 gives an idea of the structure of the information inside a GLM *.txt* file and its contents. As it can be seen it hosts many different events (rows) as arrays of information.

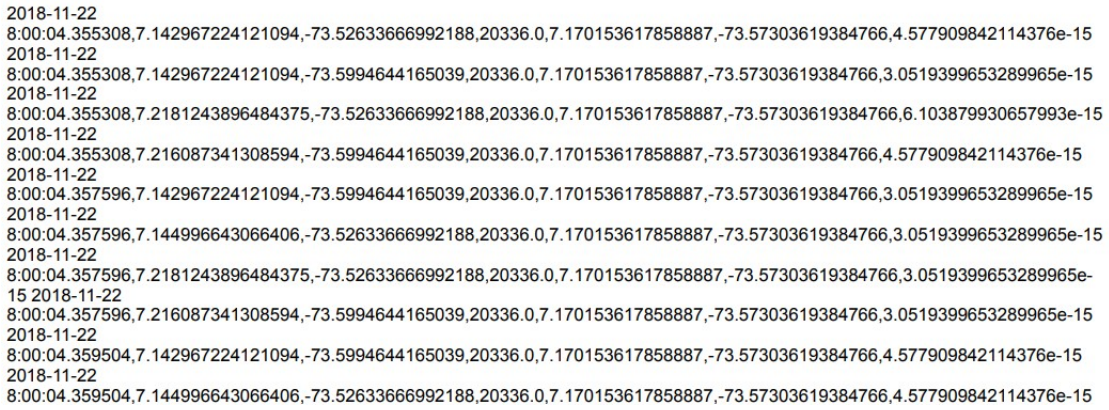

Figure 4.1: GLM data from 22nd of November of 2018 for further analysis

4.2 LMA data

Using the location of the VHF sources provided by the COL-LMA, it is possible to identify propagation of lightning leaders at different levels during lightning flashes. These sources are predominantly associated with breakdown processes of negative leaders moving through regions of positively charged cloud particles. Positive leaders that grow inside of a negative charge regions are poorly detected by VHF LMA systems, but often, these are detectable because of recoil leader processes occurring along positive leaders. The LMA data is generated by each LMA antenna in Colombia, by dumping *.dat* files every 10 minutes. Each antenna dumps its files respectively, containing information about the distance and timing of the sources detected. In order to get 3D position of each source, the post-processing algorithm of Lightning Research Group is required. This algorithm crosses the information about various antennas regarding the same time and dumps *.dat* files for every 10 minutes period, containing the position, timing, power and other values of interest of the sources detected during the period mentioned.

This crossover information may be done more or less exhaustively. For instance, the user can select to cross information from all 8 antennas. The number of antennas is the number of simultaneous, separated detections that the algorithm requires to declare a source in the respective location. More antennas will give results with less noise but the user might lose information, as some VHF emissions might be only detected by less antennas that the specified. On the other hand, too few antenna produce a very noisy result, where a lot of the declared sources may be errors or detections of other phenomena.

The LMA algorithm returns a *.txt* file containing an identifier for noise (0) and displays the sources in space and time domain, as well as other information such as their identification number, power or ξ^2 adjustment. Alongside the sources, the program can also display the events detected by GLM among others. For this project, this LMA algorithm will be used mainly to compare GLM detections between COL-LMA detections and only a part of the program applications will be executed.

Figure 4.2 gives an idea of the structure of the information inside a LMA *.txt* file and its contents. As it can be seen it hosts many different flashes (rows) as arrays of information.

```
0 02408.050829 7.3578 -74.1295 07428  0.0 +10 011111
1 02457.817806 7.2219 -74.1866 07081  2.0 +18 101111
0 02457.818289 7.0848 -73.9154 15377  0.1 +13 111101
1 02457.822605 7.2321 -74.1988 08707  0.2 +18 111110
1 02457.823193 7.2349 -74.2034 08662  0.0 +16 111111
1 02457.824324 7.2243 -74.1780 07758  0.8 +12 011111
1 02457.824642 7.2262 -74.2119 09336  1.9 +19 101111
1 02457.825658 7.2351 -74.1968 08534  0.1 +23 111111
1 02457.826386 7.2298 -74.2086 08669  0.6 +23 111110
1 02457.826472 7.2381 -74.2032 08539  0.0 +10 011111
1 02457.828477 7.2360 -74.2003 08707  0.4 +19 111110
1 02457.829698 7.2291 -74.1817 09607  0.0 +23 111110
1 02457.830219 7.2369 -74.2090 08999  0.2 +20 101111
1 02457.830873 7.2470 -74.2232 09854  0.1 +10 011111
0 02457.831726 7.0872 -73.9786 13763  0.9 +15 111110
0 02457.831922 7.2522 -74.2244 08363  2.3 +18 111011
```

Figure 4.2: LMA data from 22nd of November of 2018 for further analysis

4.3 Resolution Algorithms

The presented data can be analysed from different perspectives. Once the GLM data has been delimited, it will be compared to the COL-LMA data. To accomplish so, a set of parameters have been created in order to analyze and compare the data correlation between the two lightning locating systems. These characteristics were obtained from UPC's Lightning Research Group [10].

4.3.1 Processing Methods

A Matlab code has been developed to compare the data from COL-LMA and GLM. This algorithm examines data from both sensors and correlates them based on their time proximity. The application produces statistical results, typical value distributions or histograms, including information about such correlations. For example, a source and an event separated by less than 10 ms are regarded to be related. Because events and sources have various qualities, this relationship can be used to compare event properties with source attributes and generate distributions that allow us to analyse the performance of both sensors.

In this thesis, different parameters have been considered to analyze the performance of the GLM using the COL-LMA. These parameters are flash detection efficiency, flash false alarm candidates, flash duration and flash attributes for COL-LMA sources. For all of them, an algorithm has been developed in order to be able to extract statistical results of the provided data from both sensors at given points in time. This algorithms are also useful for creating plots to represent the overall performance.

Flash Detection Efficiency Algorithm

The Flash Detection Efficiency is the ratio of GLM detected flashes to the total number of LMA flashes. A timing and distance criterion is used to exclude out flashes that occur at various times as well as simultaneous flashes that occur at separate storms. This is a flash by flash method. LMA level 2 data is used as a reference for flashes detected by the LMA. LMA flashes will be limited to a predefined region.

Figure 4.3 is a visual representation of the data processing method for analyzing Flash Detection Efficiency from both lightning detector sensors previously described.

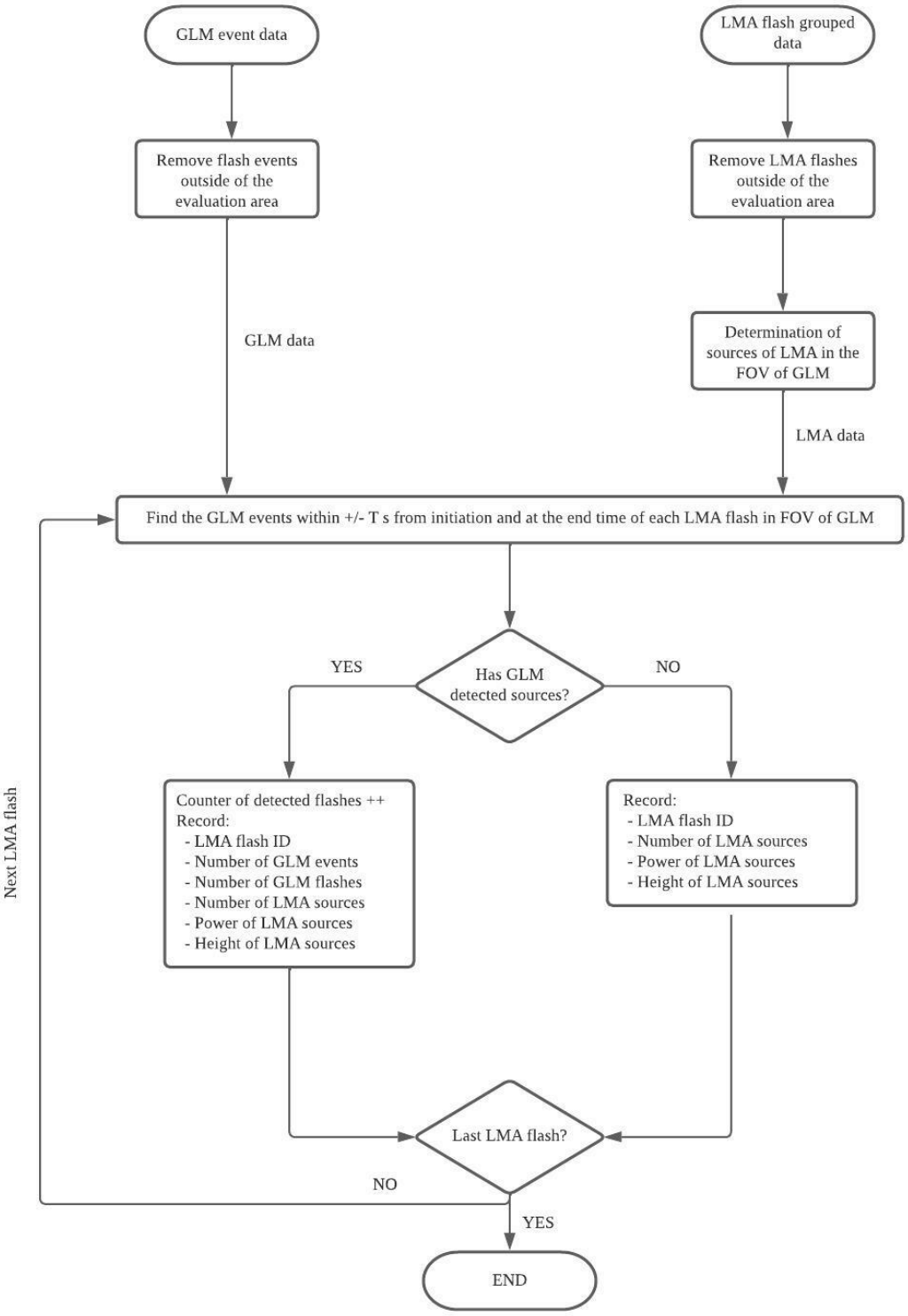

Figure 4.3: General resolution algorithm for Flash Detection Efficiency

Flash False Alarm Algorithm

The term Flash False Alarm (FFAR) refers to the detection of false LI flash detections. GLM flashes that are not matched with LMA flashes are recognized as possibilities for False Alarm in this situation (FFA). LMA source data (LMA level 1 data) will be utilized to validate erroneous detections for these candidates.

Figure 4.4 is a graphical illustration of the data processing approach used to assess Flash False Alarm candidates.

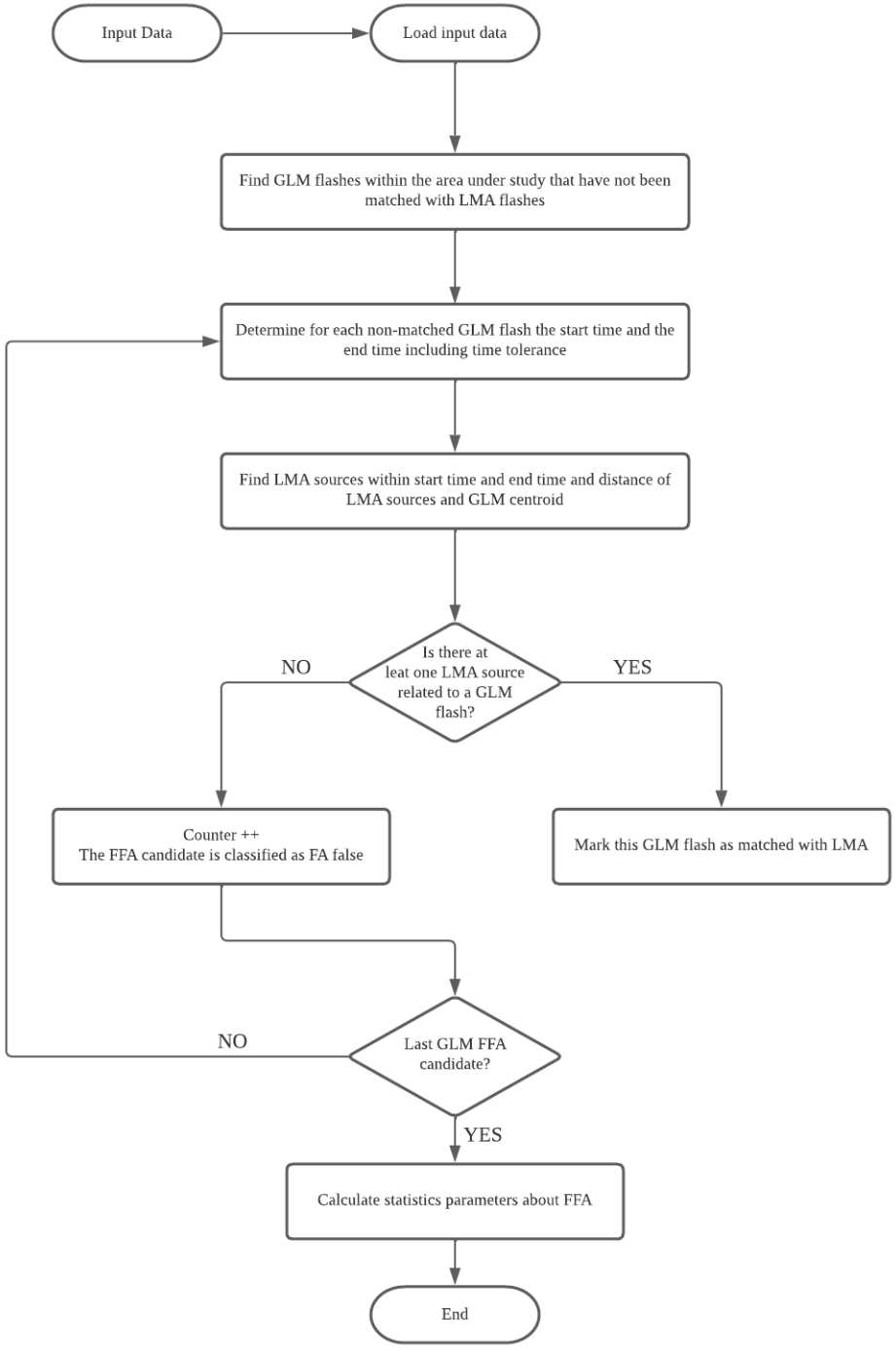

Figure 4.4: General resolution algorithm for evaluating Flash False Alarm candidates

Flash Duration Algorithm

At the flash level, time duration is calculated as the difference between the time of the first LMA flash (first source) and the time of the first event detected by GLM.

Figure 4.5 is a visual representation of the data processing method for evaluating Flash Duration.

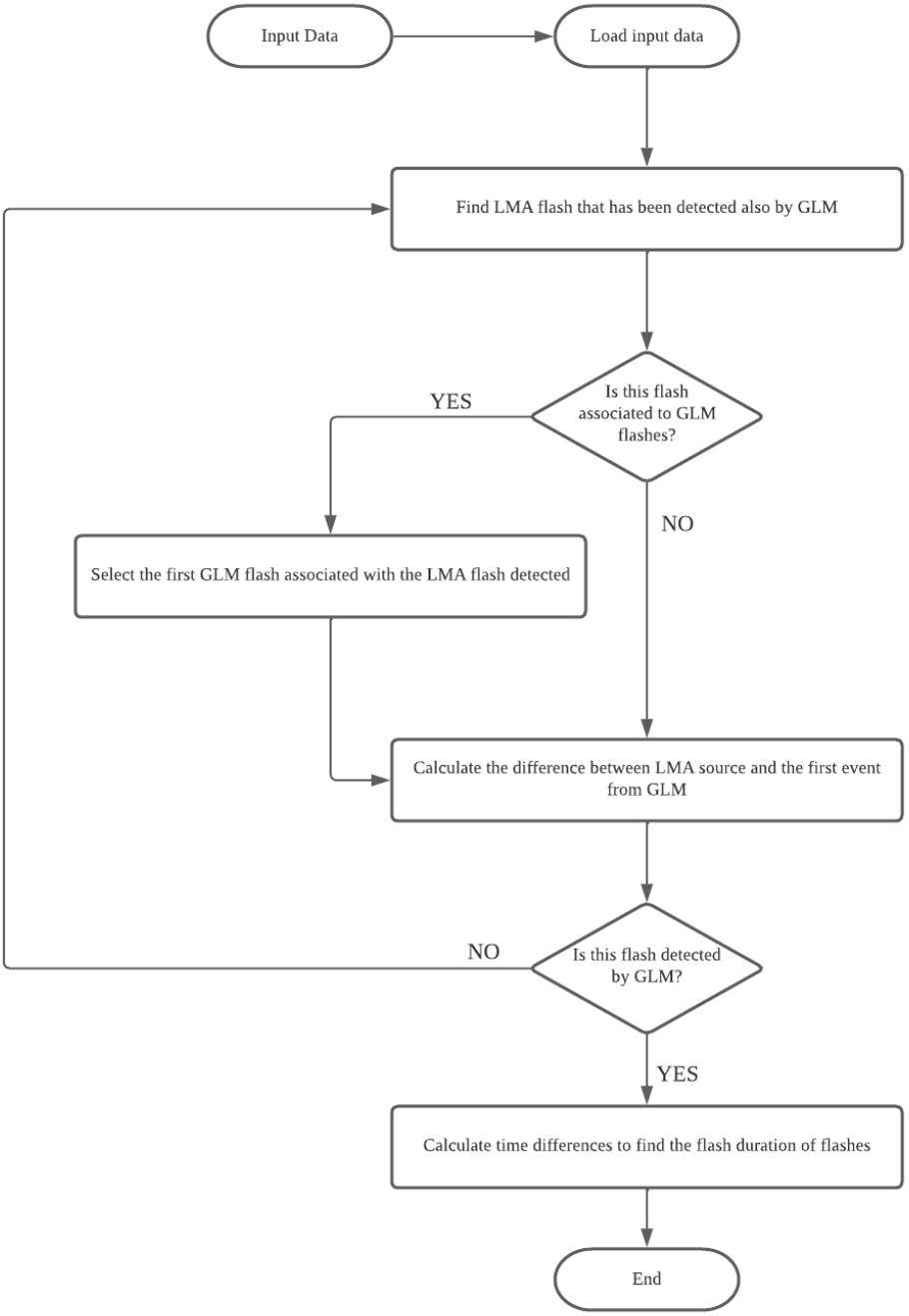

Figure 4.5: General resolution algorithm for evaluating Flash Duration

Chapter 5

Results Analysis

Important statistical data and plots for both Geostationary Lightning Mapper and Colombia Mapping Array are reported in this chapter. By analyzing simultaneous flashes detected in the same window of time the performance of each lightning detector can be described in terms of lightning flashes duration, flash size, time between flashes and flash altitudes, among other parameters.

5.1 Evaluation Case

Performance of both GLM and LMA depends on many factors. The number of lightning mapping sensors and network geometry, as well as, the gridded field of view of Geostationary Lightning Mapper are important to define the coverage range within there can be found the most indicative lightning sources. However, in order to analyse the lightning events, it is necessary to filter the flashes captured during a specific period of time by both detectors. This window of time must cluster the maximum number of captured sources

The time period during which both GLM and Colombia LMA detected several events around Barrancabermeja with high analysis potential is considered to be during the fall season of 2018, specifically, the 22nd of November of 2018. During this period, where data are available for only a maximum of 30 minutes, 1 valuable episode was recorded, that provided a huge number of detections.

On November 22, 2018, a lightning flash occurred in Barrancabermeja, Colombia, approximately, at 7.4 º latitude and 73.85 º longitude. The flash occurred in a cell of a huge nocturnal thunderstorm system within the COL-LMA coverage area near Barrancabermeja, extending from 35 to 75 km from the radar. The initial component of the flash occurred beyond the GLM sensors' Field of View in an area with cloud top temperatures ranging between 70 and 75 ºC, equivalent to heights of 14.5 km. The COL-LMA recorded a portion of the flash that developed in a less deep region with warmer cloud top temperatures of 65 to 70 ºC equivalent to heights of 13.5 km.

For later analysis, the data captured by COL-LMA is depicted in Figure 5.1 which will be used to relate features of both optical observations and high frequency detections with lightning processes and cloud properties.

5.1.1 COL-LMA data preview for case evaluation

The 30 minutes event under analysis that happen in Barrancabermeja, is being described by using a multipanel display of lightning activity detected by the COL-LMA during a time interval of the GLM covering, as can be seen in Figure 5.1. The top panel is altitude above mean sea level (km) versus time (seconds). The left panel is a plan view map and the panels at the right show altitude (km) versus latitude (top) and longitude (bottom).

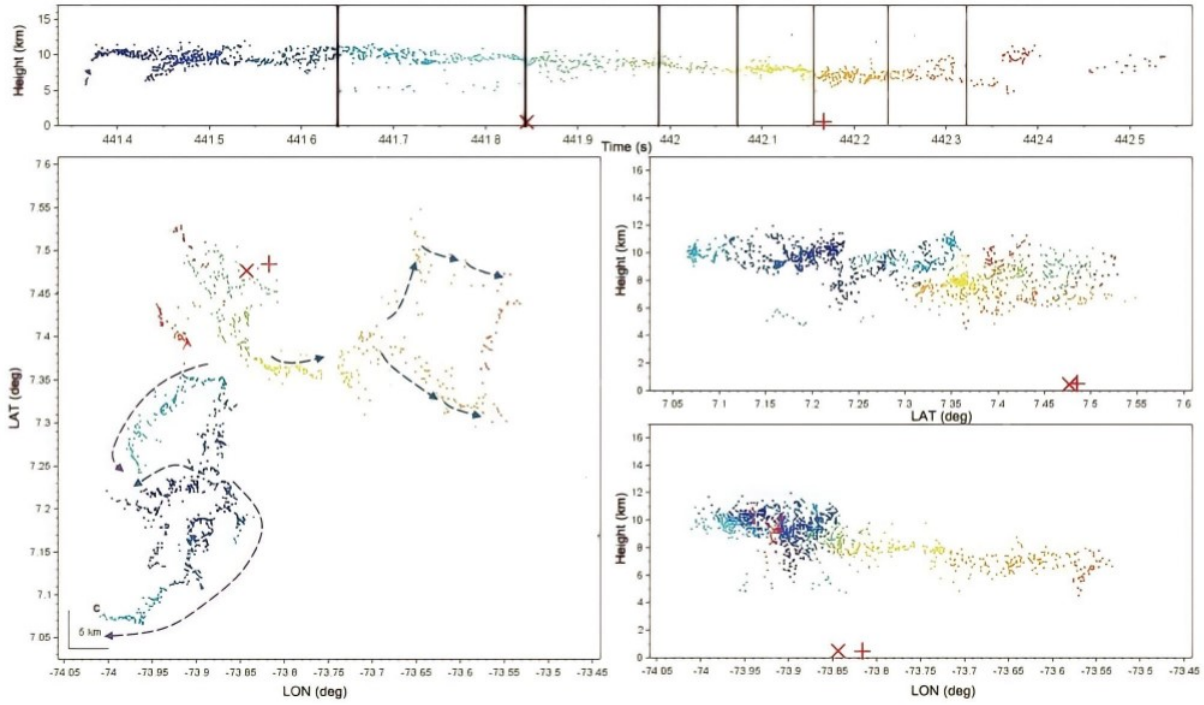

Figure 5.1: LMA data of the flash on November 22, 2018

At 7.223 º / 73.91 º, the flash began at the coldest cloud top. According to LMA data, the flash began at a height of 5 km, with a negative leader propagating upwards at roughly 105 m/s up to 11 km. After around 50 ms, fresh negative leaders emerged in the same position as the previous one and extended concurrently to the south and north for 450 ms. During this time, sources linked with positive leader breakdown were discovered at a lower altitude of 5 km. During the first 500 ms of the flash, the negative and positive leads confirmed the presence of positive polarity electric charge between 6 and 11 km altitude and negative polarity electric charge below 5 km.

Near 441.85 s, a new IC breakdown occurred at the flash's northern edge, just as a negative CG stroke of was measured. Slow negative leads stretched radially 5 km for 150 ms from the site of the CG stroke. Following this, a rapid negative leader was begun from this location and spread toward the east into a stratiform zone for around 175 ms before decreasing from 9 to 7 km altitude and branching 40 ms before terminating. Following the conclusion of this leader, a positive +CG stroke occurred near the position of the previous –CG stroke. At this moment, a quick horizontal negative leader at 7 km expanded the flash's propagation eastward. This leader had two branches that extended concurrently to the south-east and north. A branch spread quickly toward the north-east from the leader in the north.

The flash ended with the conclusion of this leader propagation, which was followed by a brief, isolated breakdown to the north-east of the two CG positions.

5.2 Evaluation of GLM using LMA as reference

In the framework of this study, the spatial and temporal lightning parameters have been analyzed conforming to a detailed examination of statistical data and plots. The parameters used to assess Geostationary Lightning Mapper (GLM) have been established accordance to the objective comparison with the COL-LMA, which is believed to be the reference network over the area of interest. The assessment relates to the conventional performance measures of lightning location systems and focuses on understanding lightning leader processes connected to GLM detections.

To identify whether a GLM flash is connected to a COL-LMA flash, both must occur at the same time and in the same area. At compare the locations, the maximum distance permitted between the centroids of both flashes is set to 50 km. A time tolerance is given to the start and finish of the flash to allow for some tolerances in the LMA flash time frame. The default value for this option is 0.1 seconds.

5.2.1 Location Accuracy

To support the Geostationary Lightning Mapper operation, the Colombia Lightning Mapping Array data has been evaluated. COL-LMA identifies sources within a certain radius of the station's center, which may vary based on the number of stations available or the orography of the surroundings. An excellent method for determining the range is to establish a grid to analyze the power detection of the COL-LMA data. The cells with the lowest power levels would represent the most sensitive places, where detection is most exact. A good range value may then be derived using the most sensitive locations found.

For this project it has been considered that the region of interest has a maximum range of 150 km in order to describe how the COL-LMA data quality is in the target area. Nevertheless, an area with a radius of 10 km is also analyzed. These areas are focused over the region of Barrancabermeja, in the upper part of the center of Colombia, as can be seen in Figure 5.2, and encompasses approximately 71000 km^2 and 315 km^2, respectively. The largest rounded area considered is delimited by the Colombian cities of Aguachica and Tunja. It is defined by latitude 8^{o} 18' 45" N, longitude 73^{o} 37' 3" W and latitude 5^{o} 32' 7" N, longitude 73^{o} 22' 04" W.

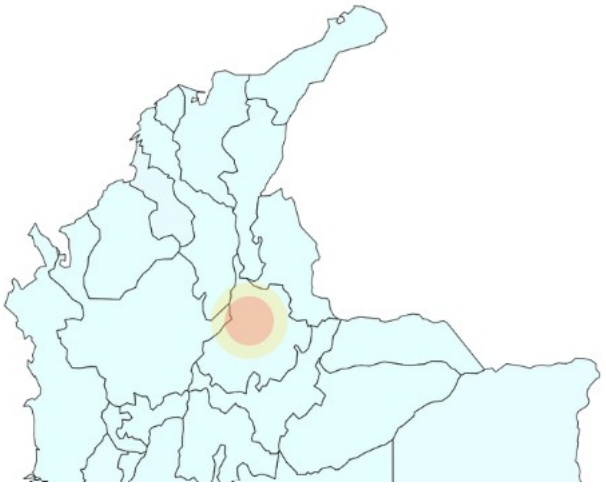

Figure 5.2: COL-LMA and GLM coverage areas (10 km radius and 150 km radius areas)

5.2.2 Sensitivity Analysis

The lightning detection sensitivity analysis focuses on the performance of the GLM based on the data from COL-LMA. It has been taking into account the case recorded on the fall of 2018, yielding evaluation of cross-correlation data between both the ground-based lightning detector and the analyzed space-based lightning detector, after knowing the individual behavior of the occurrence. Some crucial statistics will be retrieved after comparing the parameters analyzed below.

Flash Detection Efficiency

The first approach to delimit data is by evaluating the detection efficiency of events captured by GLM in relation the flash detections supplied by the COL-LMA for different constraints.

An LMA flash is considered detected by GLM if GLM records at least one event between the start and finish of the LMA flash. Moreover, because LMA flashes are used as a reference, a detection effectiveness of 100% is expected. However, distance requirement and time constraints are utilized to confirm that these GLM occurrences are from the same LMA flash. Hence, different time-space constraints will be considered in 4 different scenarios, to estimate the performance of GLM for detecting flashes.

- ***First Scenario***
  In this first scenario, all flashes within a 150 km radius, with a maximum of 50 km between centroids and the requirement of 50 sources to evaluate if a LMA flash is removed, are considered. This limits the use of high-quality LMA flashes while also removing tiny flashes.

Table 5.1: Flash detection efficiency parameters for data evaluation in the first scenario

Constraint	Value
Range	150 km
Distance between centroids	50 km
Time tolerance	0.1 s
LMA sources to accept flash	50
GLM events to accept flash	1

With the parameters established in Table 5.1 the detection efficiency can be easily calculated taking into account the data depicted in the following table, since to determine this value it is necessary to take into account the flashes recorded by GLM in relation with the flashes detected by COL-LMA.

Table 5.2: First scenario detection efficiency

GLM flashes detected	151
LMA flashes detected	151
Efficiency	100 %

The two sensors have captured the total lightning produced during the 30-minute interval under consideration. Therefor, the detection efficiency attained for this initial result is very high. All flashes assessed are correlated with a GLM flash, most likely due to the limited number of flashes and low intensity of the event, as are the flash and source rates. This scenario takes into account an extremely active episode during night time.

- ***Second Scenario***

  In this second scenario, all flashes in a range of 150 km, with a maximum of 50 km between centroides, but without a minimum number of sources per LMA flash, are considered.

Table 5.3: Flash detection efficiency parameters for data evaluation in the second scenario

Constraint	**Value**
Range	150 km
Distance between centroides	50 km
Time tolerance	0.1 s
LMA sources to accept flash	0
GLM events to accept flash	1

With the parameters established in Table 5.3 the detection efficiency can be easily calculated taking into account the data depicted in the following table, since to determine this value it is necessary to take into account the flashes recorded by GLM in relation with the flashes detected by COL-LMA.

Table 5.4: Second scenario detection efficiency

GLM flashes detected	165
LMA flashes detected	166
Efficiency	99.40 %

In order to evaluate the change of detection efficiency taking into account that the maximum range of both detectors is the same, 0 LMA sources to accept a flash have been introduced as a constraint. This implies that all detected flashes are analyzed, even if they are created by only one source.

In this second scenario, the number of the total flashes detected has grown as a result of this adjustment. However, the detection effectiveness has reduced. The number of GLM flashes captured has decreased by less than 1%, as only 1 flash captured by COL-LMA has not matched the field of view of the GLM. The number of identified flashes has not grown as much as the number of flashes examined, which might indicate that flashes with less than 50 sources are not recognized by GLM or are detected but not associated to a flash.

- ***Third Scenario***

  In this third scenario, all flashes within a 10 km radius, with a maximum of 50 km between centroides and with the requirement of 50 sources to evaluate if a LMA flash is removed, are considered. This limits the use of high-quality LMA flashes while also removing tiny flashes.

Table 5.5: Flash detection efficiency parameters for data evaluation in the third scenario

Constraint	**Value**
Range	10 km
Distance between centroids	50 km
Time tolerance	0.1 s
LMA sources to accept flash	50
GLM events to accept flash	1

With the parameters established in Table 5.5 the detection efficiency can be easily calculated taking into account the data depicted in the following table, since to determine this value it is necessary to take into account the flashes recorded by GLM in relation with the flashes detected by COL-LMA.

Table 5.6: Third scenario detection efficiency

GLM flashes detected	11
LMA flashes detected	16
Efficiency	68.75 %

The detection efficiency for flashes within a range of 10 km with minimum 50 sources to accept flash is approximately 69%. In this scenario, less flashes have been detected for both ground-based and space-based sensors. As the number of correlations decreases, these constraints becomes more restricted and affect the detection efficiency. As a result, it is possible that GLM misses certain minor flashes.

- ***Fourth Scenario***

  Finally, in this fourth scenario, all flashes in a range of 10 km, with a maximum of 50 km between centroids, but without a minimum number of sources per LMA flash, are considered.

Table 5.7: Flash detection efficiency parameters for data evaluation in the fourth scenario

Constraint	**Value**
Range	10 km
Distance between centroides	50 km
Time tolerance	0.1 s
LMA sources to accept flash	0
GLM events to accept flash	1

With the parameters established in Table 5.1 the detection efficiency can be easily calculated taking into account the data depicted in the following table, since to determine this value it is necessary to take into account the flashes recorded by GLM in relation with the flashes detected by COL-LMA.

Table 5.8: Fourth scenario detection efficiency

GLM flashes detected	15
LMA flashes detected	22
Efficiency	68.11 %

Finally, when both the range and the LMA sources considered have been changed at the same time, the detection efficiency in such a small area reduces. The number of flashes analyzed has grown as a result of the elimination of the minimum source constraint. Nevertheless, the detection efficiency has not been increased, it remains at a value similar to the third scenario with an efficiency of approximately 68%.

From a simple inspection, it can be deduced that for the episode from 22nd of November of 2018, the storm was not particularly active. The study took into account a maximum of 151 flashes in 1 episode of, approximately, 30-minutes duration. In terms of the quantity of lightning flashes detected, the event under analysis was modest. A larger number of captured flashes is reflected in a larger analysis area, since for a maximum range of 150 km, the maximum number of flashes were detected by both GLM and COL-LMA.

A LMA sources and distance criterion was employed for the Detection Efficiency assessment. Four scenarios have been considered to study the evolution of GLM detection efficiency according to COL-LMA. These cases evaluates the performance of the detectors considering different constraints: A range of 150 km or 10 km considering if there is a limitation of a minimum number of sources per LMA flash or not. In general, the detection efficiency of GLM is greater than 60% and increases as the evaluation area is also expanded. The low detection efficiency for a range of 10 km, however, may be due to the reduced area analyzed in a short period of time. Moreover, GLM masking caused by solar panels or any other conceivable parameter can influence in detection efficiency of the space-based detector.

Furthermore, it is difficult to discern uncorrelated sources in the maps for LMA sources. Time-height plots may show occasional glimpses of the undetected sources, but in the short period of time of the analysis, the data to represent it is not meaningful.

Nevertheless, since GLM events' data is analyzed on a grid, the map plot for all situations displays several events superimposed. Because uncorrelated events are grouped with correlated ones, not much information can be gleaned from them.

The maps below depict the COL-LMA and GLM detections for the 22nd of November of 2018 incidents studied in order to analyze the previously calculated parameters in a qualitative and visual way.

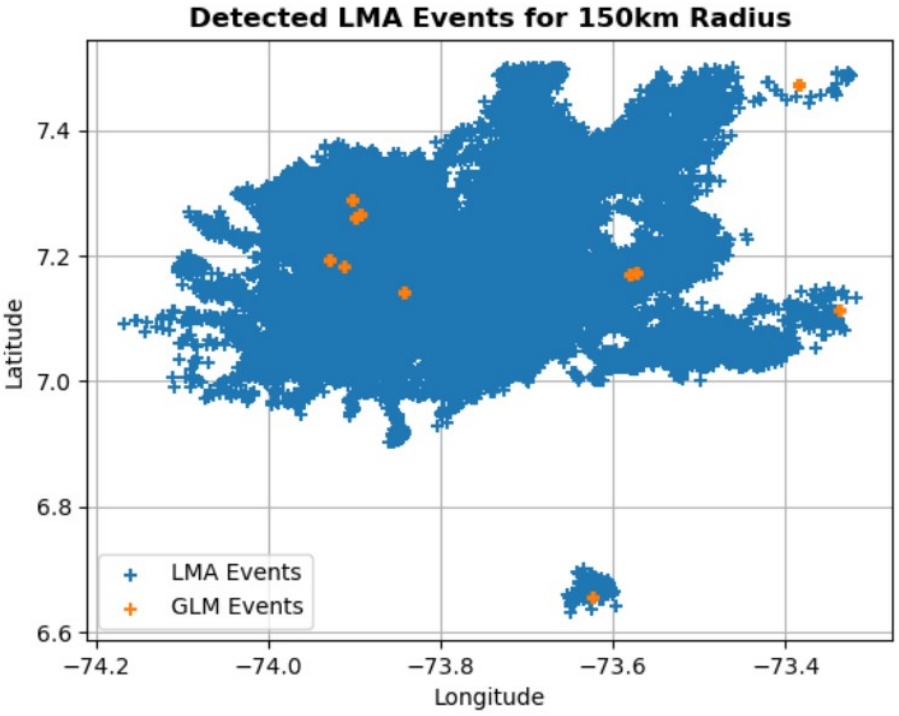

Figure 5.3: Detected GLM events for 150 km radius

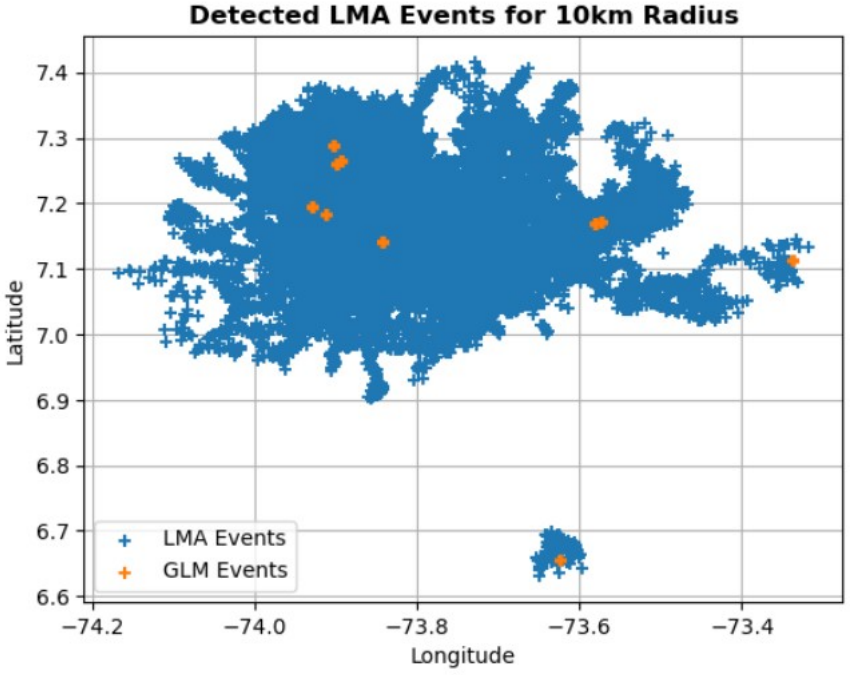

Figure 5.4: Detected GLM events for 10 km radius

Flash False Alarm

There are certain GLM events and GLM flashes in all cases analyzed that are unrelated to any LMA flash. This might happen if certain LMA flashes are not considered (due to a minimum source number constraint or severe filtering during noise reduction) or if the COL-LMA does not identify a flash. Therefore, when GLM reports a flash but LMA does not detect it, this is referred to as a Flash False Alarm (FFA) candidate.

These situations require additional attention before they can be categorized as false alarms since all the data provided by both lightning detectors must be discretized for a correct analysis of the sources and events. In order to consider that a Flash False Alarm has been captured and to analyze it independently from the general cases, it is important to verify that these incidents occur during thunderstorm bouts rather than during fair-weather, that these cases do not occur in areas of reduced detection efficiency by the COL-LMA or that these cases might be related to an existing flash but not reported by the COL-LMA due to some technical issues.

Hence, from the distribution of events and flashes captured by GLM, the not correlated ones to a COL-LMA flash have been recorded. With these data, therefore, the percentage of events and flashes can be extracted and compared with the raw LMA data. The following Table 5.9 shows the total number of flashes detected by GLM and the ones which are not correlated to LMA measurements.

Table 5.9: Flash False Alarm Candidates

	150 km	***10 km***
GLM flashes detected	151	104
GLM flashes not correlated	0	47
Percentage	0%	68.87%

Even though the uncorrelated flashes were not matched to raw COL-LMA data to determine if were true flash false alarms, the data gathered was valuable in discovering intriguing elements of the GLM flashes.

When comparing the detected and unfound flashes, the area under analysis plays an important role. For a 150 km detection range, all of the GLM flashes were detected by both sensors and none of them were associated with LMA flashes. It might be a matter of a not very active storm, since few flashes are produced in a limited region where both detectors have good performance. Therefore, both the GLM and the LMA are able to identify the flashes. For this reason the percentage of Flash False Alarm candidates are 0%. Based on these results, it is possible to deduce that Flash False Alarm parameter may also be used to calculate GLM efficiency, which in this case is 100% because all collected flashes are taken into account.

Nevertheless, for a 10 km detection range, 47 flashes were associated with several LMA flashes. It might be a matter of distance, with different LMA flashes being near enough to be assigned to their corresponding flash. This might be the consequence of analyzing an small region of LMA data with no GLM flashes observed. Hence, around 70% of the flashes can not be correlated to a COL-LMA flash and are considered Flash False Alarm candidates.

An examination of the distances obtained when the maximum distance is set to 50 km was undertaken to establish the most applicable value for the maximum distance that could be permitted to consider an LMA flash and GLM flash associated.

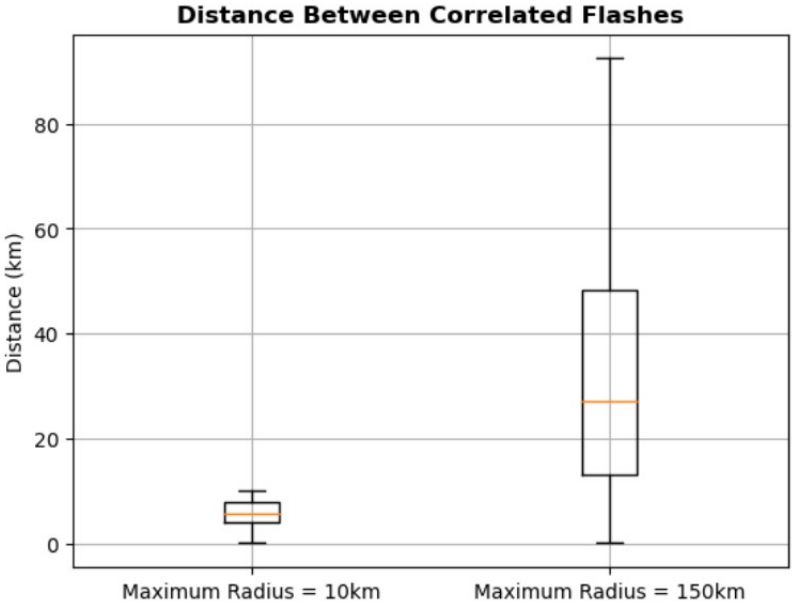

Figure 5.5: Distance between correlated flashes

In all, for the smallest region under analysis, almost all of the associated flashes are separated by less than 10 km, with a median of 6.5 km. As a result, it is reasonable to estimate that reducing the permitted distance from 50 km to 25 km would have no effect on the number of detections. For the area of 150 km radius, the distance between correlated flashes varies from 18 km to 50 km, with a median of 26.67 km.

Distribution of the Events with Height and Power

This section discusses the link between distribution of GLM events and COL-LMA sources. Some data regarding the number of sources, power, and height of the flashes have been generated in order to examine whether there are any notable variations between those COL-LMA flashes recorded and those not detected.

In terms of the association between GLM events and the height of the COL-LMA sources, Figure 5.6 shows the height of the total LMA source population in order to have a reference for the possible effect of flash height in GLM flash detection. The average height of the COL-LMA pairings is quite higher; of 9659 m above sea level.

For the analysis of the distribution of heights, the normal model has been used, since it can be justified by assuming that each observation is obtained as the sum of the independent flashes. In fact, descriptive statistics can only describe a phenomenon, without any explanation. For causal explanation, experimental design is necessary, hence the use of this statistic model is known as the correlational method.

The following Figure 5.6 shows the distribution of height of detected COL-LMA flashes for further analysis.

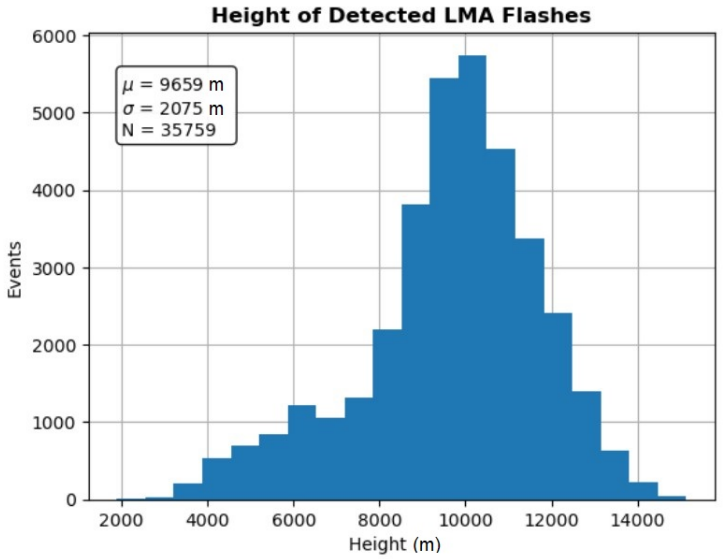

Figure 5.6: Height of detected LMA flashes

As can be seen in the Figure 5.6, 68.26% of the distribution of heights of detected LMA flashes are between 7584 m and 11734 m above sea level. Sources over 12 km and below 8 km account for 20% of the flashes detected. These results may indicate that discharges that reach into the top section of the cloud can be more easily identified by the GLM.

Finally, the distribution of power of detected LMA flashes are shown. Figure 5.7 depicts the power of the GLM-LMA pairings, which the average power is 17.06 dBW. As well as height, power distribution uses the normal model where the almost 70% of power detected is between 11.25 dBW and 22.88 dbW.

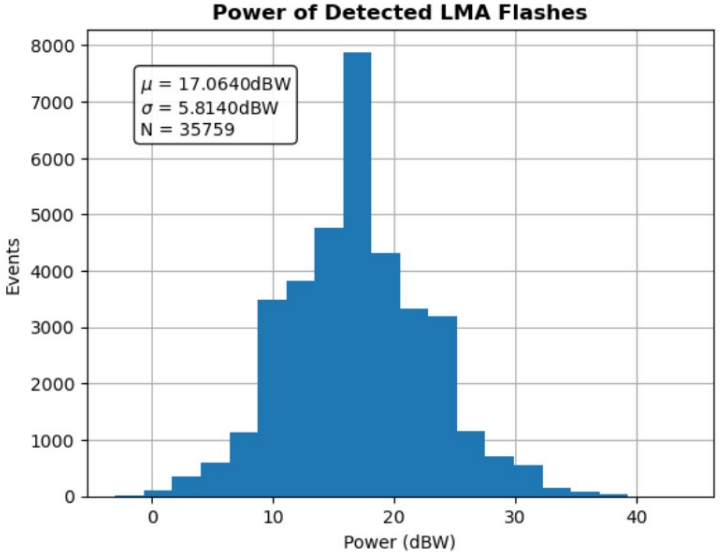

Figure 5.7: Power of detected LMA flashes

These results on the power of the sources may indicate that intense discharges which extend into the upper part of the cloud can be better detected by the GLM.

Flash Radiance

A flash recognized by GLM provides information on the emitted optical radiance in addition to duration and geographical extent. This optical lightning brightness reported by GLM may be expected to be connected to the height of the lightning channel or the power of the sources recorded by the LMA.

Nevertheless, at this point, GLM appears to have no evident link with the height of the corresponding sources identified by the LMA and due to the lack of data for longer periods of time it has not been possible to correlate in an understandable way.

A detailed examination of the brightness of the events in the context of the entire flashes will reveal a broad range of radiance in the majority of the investigated flashes. Radiance can be incorporated for the entire flash in the same manner that events are grouped into flashes. Although this reduces the sample size significantly (from events to flashes), the study on flashes may be more robust.

Flash Duration

Each lightning detectors measure optical characteristics and VHF electromagnetic waves emitted by lightning, and it is interesting to extract information about the whole flash rather than just that phenomenon. In this section, the issue for lightning duration with GLM and LMA has been addressed, by comparing simultaneous flashes between them.

The first comparison on flash duration is based on general data calculated from the whole set of observations on the incident of 22nd of November of 2018. The flash durations for both data sets are shown in the table below. A third column displays the flash duration for the sample of GLM flashes connected with LMA flashes (collocated in time and space).

Table 5.10 gathers the average time duration of detected flashes from different perspectives.

Table 5.10: Average time duration for COL-LMA and GLM flashes and correlated flashes

Parameter	**Time (seconds)**
COL-LMA flash duration	0.4338666
GLM flash duration	0.4115148
Detected LMA flash (10 km)	0.4341292
Detected LMA flash (150 km)	0.4338666

Regarding the duration of the flashes, the durations of GLM are about 20 ms shorter than the flashes detected by COL-LMA. To investigate the occurrence of the GLM events within lightning flashes, the duration of each flash has been normalized. It has been found that in most of the GLM cases, the first event is detected before the 20% of the normalized flash duration. The last GLM event occurs generally around the 85% of the normalized flash duration.

According to these results, the average length of an LMA flash is not even half that of a GLM flash. Given this knowledge, it is easy to see how GLM flashes end up matching with various LMA flashes.

Another striking feature is that related flashes have longer durations than normal flashes; this is also a highly coherent finding since the longer the flash is, the more likely it is that both systems notice it.

5.2.3 Performance analysis

The performance of GLM has been evaluated using a VHF ground-based lightning detector as reference. Several parameters have been evaluated using COL-LMA data for different coverage areas corresponding to the period of analysis with the same network configuration.

The sensitivity analysis of the GLM used the following criteria:

- Flash Detection Efficiency
- Flash False Alarm Candidates
- Distribution of the Events with Height and Power
- Flash Radiance
- Flash Duration

Regarding to these parameters some results have been obtained. Data of the lightning flash, from fall of 2018, taken from space by GLM and from the ground by the Colombia-LMA local weather radar, have been presented. This observation has offered a basis for interpreting the optical observations about lightning leader dynamics. This flash had both negative and positive strokes, as well as the presence of ongoing currents. Furthermore, weather radar data permitted calculation of the optical radiance attenuation by clouds above the lightning leaders at various positions along the route of the lightning channel propagation.

A tendency has been observed during this storm of the 22nd of November of 2018 in relation to the effectiveness of the GLM. The average flash detection effectiveness was greater than 80%. The efficiency for a 150 km radius region of analysis is very high (almost 100%), but for a 10 km radius region, the efficiency has plummeted to 68%. It has also been found that the most common way for two flashes to share a GLM flash is because different flashes are close in time and space.

Moreover, in order to see it there are any significant differences between those LMA flashes detected and not detected, some statistics for the number of sources, power and height of the flashes has been computed. In terms of the number of sources, it appears that the detected flashes have a greater number of sources. The VHF power levels observed for detected and undetected flashes are very comparable. Finally, the greatest difference between detected and undetected mean is seen in height. This disparity may imply that dense clouds on top of a lightning strike may have a significant impact on the detection of this flash from space.

Finally, in terms of flash duration values, it has been determined that LMA flashes typically last longer than GLM flashes, and the duration of correlated flashes is always longer than for the flashes analyzed individually.

Chapter 6

Environmental Impact Study

Lightning is one of the most frequently occurring geophysical phenomena. Lightning discharges in thunderstorms are an indication of the intensity of atmospheric convection which occurs under unstable atmospheric conditions, either due to the heating of the boundary layer by solar radiation during the day or by the mixing of air masses of different densities. Lightning frequencies are, therefore, related to the regions of greatest instability in the Earth's atmosphere. These regions of instability do not occur randomly around the planet, but have an organized pattern related to the climate of the Earth which is driven by differential heating of the surface by the Sun. If climate changes, the regions of convection, their intensity and hence the lightning patterns will also vary around the globe.

This chapter, assesses the importance of detecting lightning from both satellite and ground-based systems in order to predict more specific global climate models. An emphasis on the data obtained from the Geostationary Lightning Mapper and the Lightning Mapping Array over the South American region of Barrancabermeja is taken into account so as to obtain a globally and measurable vision of the major impact of climate change has in lightning and other severe weather.

6.1 Climate Change and Lightning

During the past decade, a growing body of research has emerged due to increasing concerns about impacts of climate change. These impacts are a result of changes in weather patterns that are expected to lead to an increase in the frequency and extent of natural disasters such as floods, heat waves, droughts and thunderstorms. Globally, climate change research has indicated that lightning patterns and intensity are predicted to alter with some studies indicating that global warming will increase overall lightning activity [11]. The anticipated increase in the occurrence of lightning is likely to mean more danger for society, infrastructure and the environment.

Thunderstorms are major players in the global redistribution of water substance, a key mediator of both short and long wavelength radiation. The cloud buoyancy that drives vertical motion in electrified convection results from a temperature differential of the order of 1 ^{o}C. Temperature perturbations of this order have appreciable local effects in the highly nonlinear process of cloud electrification. Temperature perturbation of this order are also clearly important in the context of global warming. Measurements of global lightning from the ground and from space have greatly stimulated the application and integration of lightning in climate studies.

6.1.1 Relationship between Lightning and Atmospheric Indicators of Climate Change

The distribution of global thunderstorms is directly linked to the Earth's climate change and, more specifically, to the general circulation of the atmosphere. The maximum solar heating at the surface in the tropics results in rising thermals and vertical mixing in the atmosphere. The area under analysis of this report is the Colombian region of Barrancabermeja, geographically located on a convergence zone with intense lightning activity. This lightning activity is positively correlated with surface temperatures over short periods of time, the increasing presence of water vapour as well as the chemistry reactions produced on the atmosphere by NO_x emissions generated by humans.

Due to the projections of a warmer climate in the future, one of the key questions is what the impact of impending global warming on lightning will be.

Temperature

Global lightning is naturally integrated by electrified weather conditions relative to the Global Earth Circuit [12]. The existence of these natural global frameworks led logically to considerations of how lightning and electrified clouds respond to temperature and temperature change. The influence of temperature from different types of radiation leads to an increase of thundercloud formation [13]. Thunderclouds are formed as the water vapors have overreached the saturation value and condenses from the evaporation of water. Thunderclouds appears because the solar heating increases the surface and lower tropospheric temperature creating an atmospheric instability, causing air to rise. It is for this reason that the more the temperature of the planet's surface increases, contributed by climate change, the formation of storm clouds and, consequently, lightning activity, also increases [14]. Different climate models support an approximate 10% increase in lightning activity for every 1 ^{o}C in global warming. [13].

Water vapour

Water vapour in the atmosphere is the primary natural greenhouse gas influencing the climate of the Earth [15]. Since water vapour absorbs infrared radiations emitted from the Earth's surface, increases in water vapour in a warmer climate would result in a positive feedback, amplifying the initial warming [16]. In general, the Earth's climate is believed to be much more sensitive to changes in water vapour in the upper troposphere, where the concentrations are naturally very low. Recently, it has been shown that thunderstorms deposit large amounts of water in the upper troposphere, moistening of the upper tropospheric environment [16], with important consequences for Earth's climate.

Hence, exist a connection between a high thundercloud coverage and lightning activity due to strong connections between lightning activity and upper tropospheric ice water content and ice crystal size. Water vapour, cloud cover, ice water content and ice particle size all have direct impacts on the Earth's radiation balance and, therefore, lightning may supply an important tool for studying the variability and changes in these important climate changes [17].

Tropospheric chemistry

Climate can also be influenced by the concentration of NO_x in the environment [18], which in a chemistry reaction between the mixture of gases present on the atmosphere causes one of the primary air pollutants, ground-level ozone, to change [19]. The contribution of anthropogenic sources to the increase of the generation of nitrogen oxides that participate in the formation of ozone, has led to the increment of greenhouse gases in the atmosphere contributing to global warming and, hence, to the increase of global temperature and lightning activity.

6.1.2 Influence of Lightning Detection Systems on Climate Change Predictions

Lightning discharges in the atmosphere owe their existence to the combination of complex dynamic and microphysical processes. Knowledge discovery and data mining methods can be used for seeking characteristics of lightning and its relation with climate change. The use of Lightning Detection Systems for forecasting meteorological parameters, related to lightning activity, can be useful for climate change evolution prediction.

During the last 50 years, various lightning mapping systems have been developed and operate at various frequency ranges and bandwidths. Ground-based detection systems using multiple antennas and satellite-based systems using a direction and a sense antenna in the same location are currently the most common types of lightning detection systems globally [20]. These networks are continuously improving, and their data are growing in importance for scientists and operational weather forecasters [21].

Lightning data gathered by either Lightning Mapping Arrays or Geostationary Lightning Mappers can be used in lightning prediction models in which data science powers the predictive capabilities [21]. In this way, the data collected by the lightning detectors can be used as a basis for machine learning algorithms that predict the evolution of lightning activity and, consequently, evaluate the progress of climate change [21].

6.2 Negative Impacts of Lightning

Lightning is a natural danger that may be fatal and devastating on short time intervals while also having significant climatic consequences on longer time scales. It is accompanied by extreme weather, hail, and flash floods, which can result in considerable economic damage. It also endangers aircraft safety and renewable energy generation via wind turbines, and it is known to have a negative impact on electric power utilities and transmission lines. These scenarios forecast a few degrees of atmospheric warming near the Earth's surface, resulting in dramatically altered climate regimes in many parts of the planet, as well as changes in the intensity and frequency of atmospheric natural catastrophes.

6.2.1 Negative Effects of Extended Lightning Activity

There are various aspects of related effects accompanying thunderstorms during severe storms, and these include tornadoes, hail and flash flooding, but there are also negative effects directly related to the actual cloud-to-ground stroke of a lightning flash that can affect human society. These are the ignition of forest fires and damages to aircraft or wind turbines that can lead to fatalities or injuries.

Forest Fires

Lightning is a major source of tree and forest damage, either immediately killing trees on impact or initiating flames and burning vast numbers of trees when circumstances are favorable for wildfire spread [22]. Wildfires have an impact on the carbon cycle through complicated feedbacks caused by changes in the forest's carbon sequestering capacity, direct emissions of volatile organic compounds and carbon dioxide (which alter clouds and precipitation), and the large-scale drop in albedo of the burnt region. The exact correlations between lightning frequency, fire incidence, and area burned are difficult to determine since various factors, such as geography and tree density, precipitation or fuel availability, influence the result of an ignition event caused by a cloud-to-ground flash [22].

Damages to aircraft

The fast rise of the aviation sector in the early twenty-first century may be linked to a number of economic and regulatory difficulties, which converted air travel into a reasonably affordable commodity for vast segments of society [23].

The increased number of routes that intersect with significant lightning generating zones exposes a large number of aircraft to lightning damage, while it is difficult to measure the proportion [23]. A full examination of lightning dangers to aircraft focuses mostly on technological reasons, such as the increased adoption of composite materials in aviation design (which makes them more susceptible to damage upon lightning strike) [13]. While in-flight damage is well recognized and operationally considered, thunderstorms, lightning, and associated weather phenomena like as hail, heavy rain, turbulence, and downbursts affect the ground segment of aviation as well. Thunderstorms and lightning pose a significant threat to airports, air traffic control centers, communication towers, and navigation beacons [13].

Damages to wind turbines

Due to the growth of renewable energies for global economy transitioning to carbon-free energy generation, more wind power stations are placed. Turbine blades revolving at several hundred meters altitude are frequently hit by lightning, causing damage to the rotor and necessitating a temporary shutdown for part replacement and maintenance [24]. Because wind farms are located in windy places, they function as triggers for direct connection of lighting to turbine blades. Electric current surges frequently bypass lightning protection mechanisms used on wind turbines, resulting in burns, punctures, tip damage, and edge debonding. As a result, energy businesses are looking for ways to reduce downtime and economic losses. The Lightning Mapping Array (LMA) is used to examine lightning strikes on wind turbines [25]. When thunderstorms were close, it was discovered that the movement of turbine blades caused electrical discharges at 3 s intervals over periods ranging from minutes to hours. The findings suggest that moving wind turbine blades frequently function as lightning triggers, increasing their own susceptibility [25].

Chapter 7

Conclusions

Lightning Mapping Arrays (LMAs) give the most complete depiction of lightning flashes. These networks have been frequently utilized in research to study lightning physics, thundercloud electrification, and thunderstorm characterisation. Aside from research applications, LMA enables real-time decimated data for operational needs. Many elements influence the LMA's performance. The number of sensors and network geometry are critical in defining the coverage range and artifacts in the source solutions. Furthermore, the noise level restricts the potential range due to the reduced capacity to detect lightning sources. Orographic factors can also restrict coverage in some areas. As a result, the LMA's performance might vary from day to day owing to a variety of factors such as differences in local noise at each station and station availability.

This performance variation leads to implement more lightning detection methods from different perspectives, such as GLM, which provides information from a geostationary orbit. Nevertheless, it is necessary to set the bases for the validation tools that will be used on this sensor. To do so, an analysis of the performance of the GLM according to the data reference from the COL-LMA has been conducted. For this, some statistical data and plots have been provided in order to be able to compare and examine the performance of the GLM. Duration, size, relation between duration and size, time between flashes and flash altitudes have been employed to generate the concluding remarks of this thesis.

The average flash detection effectiveness was in the range of 100% for ranges of 150 km, while for smaller regions of 10 km, the efficiency has plummeted below 70%. It has also been assumed that some technological issues, such as the GLM solar panel masking, are to blame for the precipitous decline. It has been demonstrated that the efficiency is sensitive to the range chosen and the constraints on the LMA data. This is mostly owing to the GLM short observation intervals, which severely limit the amount of data to be evaluated. In addition to the detection efficiency, it has been illustrated that for large ranges there are non-correlated events. However, as the area of analysis decreases almost 69% of the flashes have to be analyzed as a Flash False Alarm candidates. This confirms the necessity to use LMA sensitivity maps for each day or storm episode.

In terms of flash duration, the GLM flashes are approximately 20 ms shorter than the COL-LMA flashes detected. It has been standardized the duration of each flash to study the incidence of GLM occurrences inside lightning flashes and it has been discovered that in the majority of GLM situations, the initial event is identified before the first 20% of the normalized flash duration. The last GLM event usually occurs at 85% of the normalized flash duration. All

correlated flashes lasts longer than the ones that are not.

Moreover, it has been shown that the height and power distribution of the flashes captured by the ground-based sensor and the GLM can be analyzed using the properties of the GLM. The average height of flashes is approximately 9.7 km and the mean value of the power emitted by these flashes is 17 dbW. It has also been considered that lightning at higher altitudes offers better circumstances for GLM detection, although there is no direct relationship between LMA sources or leader processes and optical emissions. This will constrain the GLM pulse level analysis.

To continue the work done in this research, it would be interesting to evaluate the flash detection efficiency using GLM as a reference since GLM flashes could be assigned to more than one flash.

It would also be interesting to continue analyzing the time length of flashes and maybe groups in order to have a better understanding of the temporal relationship between the LMA and GLM flashes and groups. This might aid in determining which data should be utilized as a reference for evaluating detection efficiency.

Bibliography

1. UMAN, Martin A. *The lightning discharge*. Courier Corporation, 2001.
2. COORAY, Vernon. *An introduction to lightning*. Springer, 2015.
3. RYCROFT, M.J; ISRAELSSON, S; PRICE, C. The global atmospheric electric circuit, solar activity and climate change. *Journal of Atmospheric and Solar-Terrestrial Physics*. 2000, vol. 62, no. 17, pp. 1563–1576. ISSN 1364-6826. Available from DOI: https://doi.org/10.1016/S1364-6826(00)00112-7.
4. COORAY, G Vernon. *The lightning flash*. Iet, 2003. No. 34.
5. COORAY, Vernon. *Lightning Electromagnetics*. The Institution of Engineering and Technology, 2012.
6. MONTANYÀ, Joan; VELDE, Oscar van der; WILLIAMS, Earle R. The start of lightning: Evidence of bidirectional lightning initiation. *Scientific Reports*. 2015, vol. 5, no. 1, pp. 1–6.
7. RAKOV, Vladimir A; UMAN, Martin A. *Lightning: physics and effects*. Cambridge university press, 2003.
8. NOAA, National Oceanic Atmospheric Administration. *Instruments: Geostationary Lightning Mapper*. Available also from: https://www.goes-r.gov/spacesegment/glm.html.
9. LÓPEZ, Jesús A.; MONTANYÀ, Joan; VELDE, Oscar van der. Initiation of lightning flashes simultaneously observed from space and the ground: Narrow bipolar events. *Atmospheric Research*. 2022, vol. 268, p. 105981. ISSN 0169-8095. Available from DOI: https://doi.org/10.1016/j.atmosres.2021.105981.
10. MONTANYÀ, J; VELDE, OA van der; PINEDA, N; LÓPEZ, JA. ISS-LIS data analysis based on LMA networks in Europe. 2019.
11. MAHOMED, Maqsooda; CLULOW, Alistair D; STRYDOM, Sheldon; SAVAGE, Michael J; MABHAUDHI, Tafadzwanashe. Lightning monitoring and detection techniques: Progress and challenges in South Africa. *South African Journal of Science*. 2021, vol. 117, no. 1-2, pp. 1–7.
12. RYCROFT, MJ; ISRAELSSON, Sven; PRICE, Colin. The global atmospheric electric circuit, solar activity and climate change. *Journal of Atmospheric and Solar-Terrestrial Physics*. 2000, vol. 62, no. 17-18, pp. 1563–1576.
13. WILLIAMS, ER. Lightning and climate: A review. *Atmospheric research*. 2005, vol. 76, no. 1-4, pp. 272–287.
14. PATEL, Akash D. *Modulation of African lightning and rainfall by the global five day wave*. 2001. PhD thesis. Massachusetts Institute of Technology.
15. DEL GENIO, Anthony D. The dust settles on water vapor feedback. *Science*. 2002, vol. 296, no. 5568, pp. 665–666.

16. RIND, David. Just add water vapor. *Science*. 1998, vol. 281, no. 5380, pp. 1152–1153.
17. SHERWOOD, Steven C; PHILLIPS, Vaughan TJ; WETTLAUFER, JS. Small ice crystals and the climatology of lightning. *Geophysical Research Letters*. 2006, vol. 33, no. 5.
18. OTT, Lesley E; PICKERING, Kenneth E; STENCHIKOV, Georgiy L; HUNTRIESER, Heidi; SCHUMANN, Ulrich. Effects of lightning NOx production during the 21 July European Lightning Nitrogen Oxides Project storm studied with a three-dimensional cloud-scale chemical transport model. *Journal of Geophysical Research: Atmospheres*. 2007, vol. 112, no. D5.
19. GREWE, Volker. Impact of climate variability on tropospheric ozone. *Science of the total environment*. 2007, vol. 374, no. 1, pp. 167–181.
20. RUDLOSKY, Scott D; FUELBERG, Henry E. Documenting storm severity in the mid-Atlantic region using lightning and radar information. *Monthly weather review*. 2013, vol. 141, no. 9, pp. 3186–3202.
21. MENG, Qing; YAO, Wen; XU, Liangtao. Development of lightning nowcasting and warning technique and its application. *Advances in meteorology*. 2019, vol. 2019.
22. LATHAM, Don; WILLIAMS, Earle. Lightning and forest fires. In: *Forest Fires*. Elsevier, 2001, pp. 375–418.
23. IATA. *IATA, International Air Transport Association 2022 20 year forecast*. 2017. Available also from: `http://iata.org/publications/store/Pages/20-yearpassenger-forecast.aspx`.
24. RACHIDI, Farhad; RUBINSTEIN, Marcos; MONTANYA, Joan; BERMÚDEZ, José-Luis; SOLA, Rubén Rodrıguez; SOLÀ, Glòria; KOROVKIN, Nikolay. A review of current issues in lightning protection of new-generation wind-turbine blades. *IEEE Transactions on Industrial Electronics*. 2008, vol. 55, no. 6, pp. 2489–2496.
25. MONTANYÀ, Joan; VAN DER VELDE, Oscar; WILLIAMS, Earle R. Lightning discharges produced by wind turbines. *Journal of Geophysical Research: Atmospheres*. 2014, vol. 119, no. 3, pp. 1455–1462.